Master Thesis

Comparison of Sucker Rod String Design Methods, Types and Applications

OMV Petrom

Written by:
Tomuz Alina, BSc

M1535431

Advisor:
Univ.-Prof. Dipl.-Ing. Dr.mont. Herbert Hofstätter
Dipl.-Ing. Dipl.-Ing. Dr.mont. Clemens Langbauer
Dipl.-Ing. Dr. Stefan-Liviu Firu

Leoben, 08.02.2018

EIDESSTATTLICHE ERKLÄRUNG

Ich erkläre an Eides statt, dass ich die vorliegende Diplomarbeit selbständig und ohne fremde Hilfe verfasst, andere als die angegebenen Quellen und Hilfsmittel nicht benutzt und die den benutzten Quellen wörtlich und inhaltlich entnommenen Stellen als solche erkenntlich gemacht habe.

AFFIDAVIT

I hereby declare that the content of this work is my own composition and has not been submitted previously for any higher degree. All extracts have been distinguished using quoted references and all information sources have been acknowledged.

Kurzfassung

Die Verwendung von Gestängetiefpumpen als bevorzugte Fördermethode für nicht erruptiv fördernde Erdölsonden wurde mit den Jahren immer bedeutender. Durch technische Weiterentwicklungen und immer anspruchsvolleren Betriebsbedingungen setzen sich diese Fördersysteme als die am felxibelsten Ölfördermethoden weltweit durch. Einer der wichtigsten Bestandteile in der Gestängetiefpumpenoptimierung ist das Design des Tiefpumpengestänges selbst. Die Funktionalität dieses mechanischen Bauteils hat einen essentiellen Einfluss auf die Effizienz der Erdölförderung. Dessen Versagen würde zweifellos zu einem totalen Produktionsverlust führen und einen negativen Einfluss auf die Leistungskennzahlen (KPI) haben. Ein gut durchdachtes Pumpgestängendesign sichert nicht nur gute Betriebsbedingungen sondern kann ebenfalls die gesamten Produktionskosten signifikant senken. Diese Masterarbeit beschäftigt sich mit einer Analyse der am häufigsten verwendeten Gestänge- Auslegungen, sowie einer statistischen Analyse von Pumpgestänge- Versagen der letzten 3 Jahre innerhalb der OMV Petrom. Inkludiert ist des Weiteren eine Zusammenfassung von Designbesonderheiten der heutzutage verwendeten neuen Installationen, wie Fieberglas und durchgehender Pumpgestänge. Schwerpunkt dieser Arbeit ist die Erarbeitung einer Designmethoden Entscheidungsmatrix, welche es ermöglichen soll Entscheidungshilfen zu liefern bezüglich der verschieden Pumpgestängen- Auslegen die aktuell auf dem Markt verfügbar sind. Berücksichtigt werden dabei die Besonderheiten der Bohrung (Tiefe des Pumpensitzes, Inklination, Pumpengeschwindigkeit) als auch die Genauigkeit und Performance der Fördermethoden unter jeweils vorherrschenden Bedingungen.

Abstract

The application of sucker rod systems as a preferred artificial lift method and became even more defined over the years, due to technological advancements and more severe operating conditions, but managed to remain the most widely used type of oil well production all over the world. One of the most vital parts of Sucker Rod Pumping system optimization is the sucker rod string design. The performance of this piece of mechanical equipment has an essential impact on the fluid lifting efficiency. Its failure will unquestionably lead to a total loss of production and have a negative impact on the key performance indicators (KPI). A properly designed rod string not only assures good operating conditions but can significantly reduce overall production costs as well. This Master Thesis will provide an analysis of the most commonly used design methods, as well as a statistical analysis of rod failures in OMV Petrom over the past 3 years. It will also include an overview of design particularities of the special rod types used nowadays – fiberglass rods and continuous rods. The ultimate scope is providing a design method decision matrix that will facilitate the choice between the multiple design methods present on the market, considering the particularities of the well (pump setting depth, inclination, pumping speed) as well as the accuracy and performance of the methods in given conditions.

List of Tables

Table 4.1: Material parameters used in the Goodman formula [20, p. 2] 27

Table 4.2: Basic assumptions used for the calculation of taper percentages published in API RP 11L after Neely [2, p. 168] 33

Table 4.3: The main assumptions behind the Sucker-Rod String Design Methods 41

Table 6.1: Quality Criteria for the TOPSIS analysis 53

Table 6.2: TOPSIS ranking of the sucker-rod design methods based on the defined criteria 54

Table 9.1: Well operational data 63

Table 9.2: Sucker-rod string design results 63

Table 9.3: Well operational data 66

Table 9.4: Sucker-rod string design results 67

List of Figures

Figure 1.1: Number of different oil well installations in OMV Petrom, Romanian sector (courtesy of OMV Petrom) 2

Figure 2.1: The components of a sucker-rod pumping system [2, p. 60] 5

Figure 2.2: Qualitative performance curves for NEMA D electric motors [2, p. 239] 6

Figure 2.3: Schematic drawing of a double-reduction gear reducer [2, p. 227] 7

Figure 2.4: The structural parts of a common conventional pumping unit [8] 8

Figure 2.5: Wellhead arrangement of a typical sucker-rod pumping well [2, p. 195] 8

Figure 2.6: Schematic description of the pumping cycle [9, p. 12/163] 9

Figure 2.7: Construction details of a sucker-rod pin end [12] 10

Figure 2.8: The four-part modified API connection [2, p. 133] 11

Figure 2.9: Comparison of the geometry and stress distribution in the API connection (left) versus a premium Tenaris connection (right) [14, p. 27] 12

Figure 2.10: Comparison of the contact loads acting on the tubing [15, p. 3] 13

Figure 2.11: Comparison of rod-tubing contacts for coupled rods and Corods [2, p. 139] 13

Figure 2.12: Schematics of an end connector for fiberglass sucker rods [2, p. 141] 14

Figure 3.1: Hypothetical dynamometer card, if only the static loads were considered 18

Figure 3.2: Forces acting on rod element [2, p. 275] 19

Figure 3.3: Rod weight and mechanical friction in a straight section of an inclined well [2, p. 301] 21

Figure 4.1: Modified Goodman diagram for allowable stress and range of stress for sucker rods in non-corrosive service [21, p. 3] 27

Figure 4.2: Comparison of the modified Goodman diagram valid for different rod materials [2, p. 159] 28

Figure 4.3: The modified Goodman diagram for various steel grades [2, p. 157] 29

Figure 4.4: West's design procedure algorithm [2, p. 164] 31

Figure 4.5: Comparison of API taper lengths with those calculated by Neely's method [2, p. 168] 33

Figure 4.6: Algorithm for calculating rod string taper lengths with the Gault-Takacs method [2, p. 172] 36

Figure 4.7: Illustration of the design procedure [20, p. 5] 38

Figure 4.8: Serensen - Kinasoshvili diagram [1, p. 135] 39

Figure 4.9: Mechanical models of sucker-rod strings [22, p. 347] 43
Figure 4.10: Effect of mechanical resonance on plunger stroke length [22, p. 348] 45
Figure 4.11: Pump stroke amplification as a function of speed and fluid load [22, p. 349].....46
Figure 5.1: Distribution of Sucker-Rod String System failures in OMV Petrom for 2016.....47
Figure 5.2: Typical tensile and fatigue failures of a sucker rod body [2, p. 179] 48
Figure 5.3: Sucker-Rod String failure reasons within the OMV Petrom in 2016 49
Figure 5.4: Distribution of Sucker-Rod String Failures within OMV Petrom in 2016 50
Figure 5.5: Rod Connection Failure Distribution within OMV Petrom in 2016 50
Figure 5.6: Rod Body Failure Distribution within OMV Petrom in 2016 51
Figure 5.7: MTBF dynamics in OMV Petrom over the last 7 years.....52
Figure 6.1: The TOPSIS analysis results for a shallow well application 55
Figure 6.2:The TOPSIS analysis for a deep, inclined well application.....55
Figure 9.1: Sucker-rod string design diagram 64
Figure 9.2: Rod stresses for well 1 plotted on the modified Goodman diagram given by different design methods 65
Figure 9.3: Relative length of the sucker rod string tapers, compared with the main stresses - comparison of design methods.....66
Figure 9.4: Sucker-rod string design diagram 68
Figure 9.5: Rod stresses for well 1 plotted on the modified Goodman diagram given by different design methods 69
Figure 9.6: Relative length of the sucker rod string tapers, compared with the main stresses - comparison of design methods.....70

Abbreviations

ALS	Artificial Lift Systems
MTBF	Meantime Between Failures
RF	Recovery Factor
GLR	Gas-Liquid Ratio
SRP	Sucker-Rod Pump
API	American Petroleum Institute
NEMA	National Electrical Manufacturers Association
SPM	Strokes per minute
DLS	Dog Leg Severity

Table of contents

Page

1 **INTRODUCTION** **1**

1.1 Sucker Rod Pumping 1

1.2 Problem Statement 2

2 **THE SUCKER-ROD PUMPING SYSTEM** **5**

2.1 Surface Equipment 6

2.2 Downhole Equipment 9

2.3 The Sucker-Rod String 10

2.3.1 Solid steel rods 10

2.3.2 Continuous rods 12

2.3.3 Fiberglass sucker-rods 14

3 **UNIFIED MODEL OF THE PUMPING SYSTEM** **16**

3.1 Rod Loads 16

3.1.1 Static loads 17

3.1.2 Dynamic loads 18

3.2 The Wave Equation as applied to Rod Pumping 19

3.3 Unified Mathematical Model of the Pumping System 22

4 **SUCKER-ROD STRING DESIGN METHODS** **26**

4.1 Early simplified designs 28

4.2 Designs considering dynamic loads 30

4.2.1 West's method 30

4.2.2 Neely's method 32

4.2.3 API taper design 32

4.2.4 The Gault-Takacs method 34

4.2.5 Takacs – Gajda enhanced design model 36

4.2.6 Method used in OMV Petrom 39

4.2.7 The RodStar model 41

4.3 Design methods comparison 41

4.4 Special rod type design particularities 43

5 **ROD STRING FAILURES** **47**

5.1 Types of failure 47

5.1.1 Rod Body Failures 48
5.1.2 Joint failures....49
5.2 Failure statistics within OMV Petrom 49
5.3 Impact of failures on Key Performance Indicators 51
6 **TOPSIS ANALYSIS 53**
7 **CONCLUSION 57**
8 **REFERENCES....59**
APPENDICES 63
Appendix A: Sucker rod design simulation results 63

1 Introduction

Designing a well's production system is a complex activity with multiple implications in the overall field development dynamics. The selected production system must guarantee an adequate rate dynamic per established production decline while operating at the minimum cost. Optimization of the selection process is achieved only if the key technical and economic factors of the production process are defined correctly.

During the early days of life, a well usually has enough energy to drive its production fluids to the surface. As field development progresses, and the reservoir pressure declines, an energy boost must be provided, either by means of Artificial Lift Systems (ALS), or methods that target pressure maintenance, or both.

To choose the production system which will subsequently provide high production rates with low to medium initial investment and operating costs, and ensure the largest possible meantime between failures (MTBF), the following parameters are considered crucial [1, pp. 10-12]:

- Reservoir conditions (pressure, temperature, productivity index);
- Type of production fluid (oil, gas, water) and impurities content (corrosive, abrasive, waxy, etc.);
- Gas-liquid ratio (GLR);
- Recovery method(s);
- Setting depth, perforated interval and wellbore geometry;
- Costs related to the installation and operation of the system;
- Complexity of the system design and calculations;
- Conversance of the operating staff with the system;
- Available surface area and restrictions related to noise, chemicals, dimensions, etc.;
- Adaptability to an automation system;
- Intervention duration and difficulty;
- System flexibility to changing reservoir parameters.

1.1 Sucker Rod Pumping

The first and, for a long time, the only artificial lift system the engineers turned to was sucker-rod pumping. However, due to the introduction of many other lift methods, and as wells became deeper and more crooked, the application of sucker rod became more defined, whilst remaining the most widely used type of oil well production all over the world.

There are no reliable estimates on the distribution of each artificial lift method in the different parts of the world. However, the chart in Fig. 1.1, presents the share of different oil well installations within Romanian sector of OMV Petrom. With a defining majority of 70%, sucking-rod systems represent the keystone in oil production of the company, thus, invoking systems' optimization as one of the company's primary objectives.

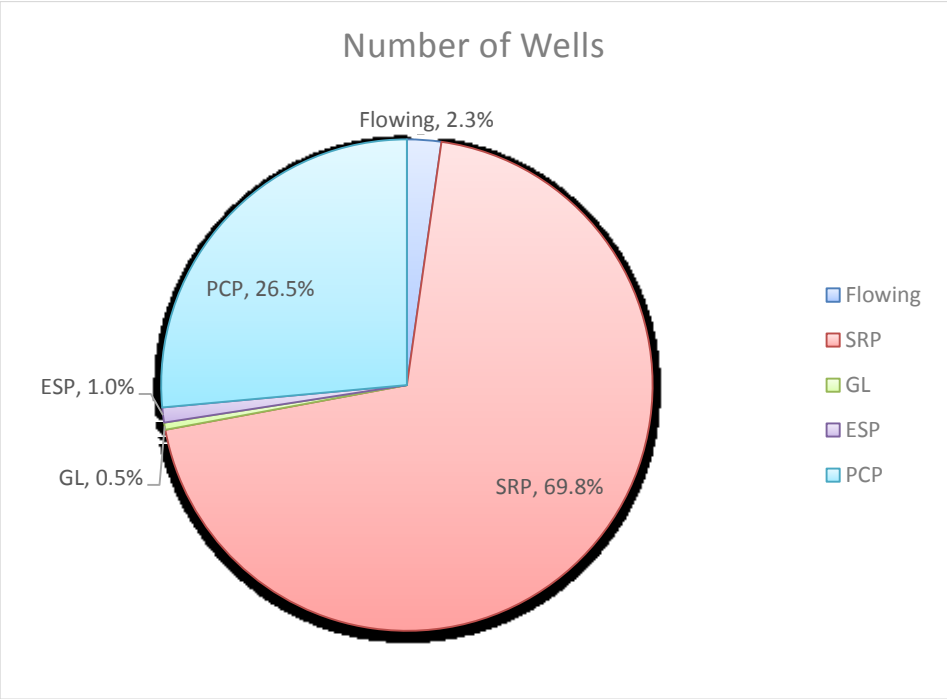

Figure 1.1: Number of different oil well installations in OMV Petrom, Romanian sector (courtesy of OMV Petrom)

The primary reason behind this high number of wells produced by SRP is the reservoirs, which being produced from mid years of the last century, are in most cases depleted. Also, the long history of SRP operation in this region promoted the familiarity of the personnel with the equipment, a decisive advantage in this case. This, and the fact that the system is easy to design, flexible to the changing reservoir conditions and simple to analyze and repair, determines the foremost use of this artificial lift method.

1.2 Problem Statement

One of the most vital components of Sucker Rod Pumping system optimization is the sucker rod string design. The performance of this piece of mechanical equipment, which due to its geometry behaves as a perfect slender bar, has an essential impact on the fluid lifting efficiency. Its failure will unquestionably lead to a total loss of production and have a negative impact on the key performance indicators (KPI). A properly designed rod string not only assures good operating conditions but can significantly reduce overall production costs as well.

During a complete pumping cycle, the sucker rod string is exposed to a combination of static and cyclic loads, as well as inertial forces, which must be considered in any design calculations to avoid failures and maximize system efficiency.

The main objectives of the rod string design are [2, p. 143]:

- The rod sizes;
- The optimum length of individual taper sections;
- The proper rod material.

At the time of designing the rod loads cannot be entirely projected, partly because they also depend on the length and size of the tapers which are about to be calculated. Hence, some approximations need to be applied to find out the potential loads that will occur during pumping.

The early rod string design methods all relied on the assumption that the sucker-rod string was subject to a simple tension loading [2, pp. 161-162]. The design principle was based on keeping the rod stress at a value based on a percentage of the tensile strength of the rod material. The quite obvious drawback of this design was its obliviousness to dynamic loads, which would result in fatigue failure of the rod joints subjected to cyclic loading.

The first one to address this essential issue in rod string design was West [3, pp. 68 - 77]. His design method attains to have the same ratio of maximum stress to allowable stress in each taper section. The loads considered in this design procedure were the rod weight in air, fluid loads and a dynamic force. To account for friction forces, he overlooked buoyancy effects, as these two usually act in opposite direction. The design of taper lengths involves an iterative process and is limited to the calculation accuracy, though giving reasonable results for small pumps and medium pumping depths.

Later, Neely [4, pp. 58-66] introduced the design concept for equal "modified stress" at the top of each taper section. The loads on the individual taper sections were calculated based on several simplifying assumptions, such as the empirical formula to calculate the maximum dynamic load, equal rod stresses on the upstroke and downstroke and linear variation of dynamic forces. This design procedure encountered for buoyancy but did not include rod friction, therefore, resulted in the taper designs which were not accurate enough.

The American Petroleum Institute (API) adopted the rod string method proposed by Neely, including in later editions of RP 11L [5, pp. 8-10] the rod percentages calculated by this method, as a sole function of pump size. Yet, the simplifying assumptions used by Neely, in addition to some basic assumptions used for calculation of taper percentages in RP 11L, enforced serious limitations on the use of this easy and time saving design procedure [2, p. 168]. The use of this shortcut method was therefore unnecessary as the computing power development permitted prioritization of accuracy against simplicity when it comes to sucker rod string design.

A more theoretically thorough design method was developed by Gault and Takacs [6, pp. 4-8], which attempts to achieve the same degree of safety in every taper section, thus, a uniform level of fatigue loading all along the string. This would be the first method to consider the effects of force wave reflections that take place in the rod string in the load calculations. It is an iterative procedure and requires more computational time than, for example, the API method, but gives reasonably accurate results.

The commercial computer program package RodStar [7, pp. 60-68] incorporates the design of the rod string in the overall analysis of the rod-pumping system. This design procedure uses predicted rod loads that result from the solution of dampened wave equation. The taper lengths are determined iteratively so that their loading is identical at the top of each taper.

The typical failure cause of the sucker-rod strings is a consequence of the type of loading and is mostly fatigue failure. Therefore, the selected design procedure must consider the cyclic nature of rod loading so that the string will withstand fatigue. In deviated wells, the friction forces play a crucial role in the string's lifespan, yet, they are being ignored or underrated in the earlier design procedures. This Master Thesis will provide an analysis of the most commonly used design methods, as well as a statistical analysis of rod failures in OMV Petrom over the past 3 years.

As Sucker-Rod Pumping systems are being pushed to their operational limits, into deeper fields and more aggressive environments, the sucker-rod string has been found as one of its weakest links. Failure statistics endorse the coupled connection to be the common cause of problems in field operations, which fail either due to inferior fatigue resistance or overloading.

The joints in the sucker rod string are subject to severe operational conditions, and can create difficulties, especially in deviated wells, where due to the concentration of side loads, the couplings can erode the tubing. Joints are also sensitive to improper initial makeup and more susceptible to fatigue failures then the rod body. These problems have found a solution since the application of continuous rod string, which inherently eliminates all the risks associated with sucker-rod joints. They also present advantages in deviated boreholes, where, due to their semi-elliptical cross-section, contact area between the rods and the tubing is increased, resulting in less downhole friction [2, pp. 137-140].

Steel rods have some common drawbacks which nowadays can be overcome with special rod types. They have relatively high weight, which increases the power needed to drive the pump and reduces the depth of Sucker-Rod pumping application. Moreover, most of the steel types that rods are made of are susceptible to corrosion damage in well fluids. Corrosion resistance of steel rods can be achieved by using high quality alloys, which will significantly increase the capital costs. These problems are disregarded using relatively new to the industry fiberglass-reinforced plastic sucker rods. These rod types, however, require specific design requirements, which will be acknowledged in this Master Thesis.

The ultimate scope of this Master Thesis is providing a design method decision matrix that will facilitate the choice between the multiple design methods present on the market, considering the particularities of the well (pump setting depth, inclination, pumping speed) as well as the accuracy and performance of the methods in given conditions.

2 The Sucker-Rod Pumping System

The sucker-rod pumping system is made up from several components, conventionally divided in:

- Surface equipment – including the prime mover, the gearbox, the pumping unit (walking beam and horsehead), the polished rod and the wellhead assembly;
- Downhole equipment – including the rod string, the positive displacement pump (pump plunger and barrel), and the downhole gas separator (if required).

These elements are emphasized in the Fig. 2.1, showing a common pumping system installation.

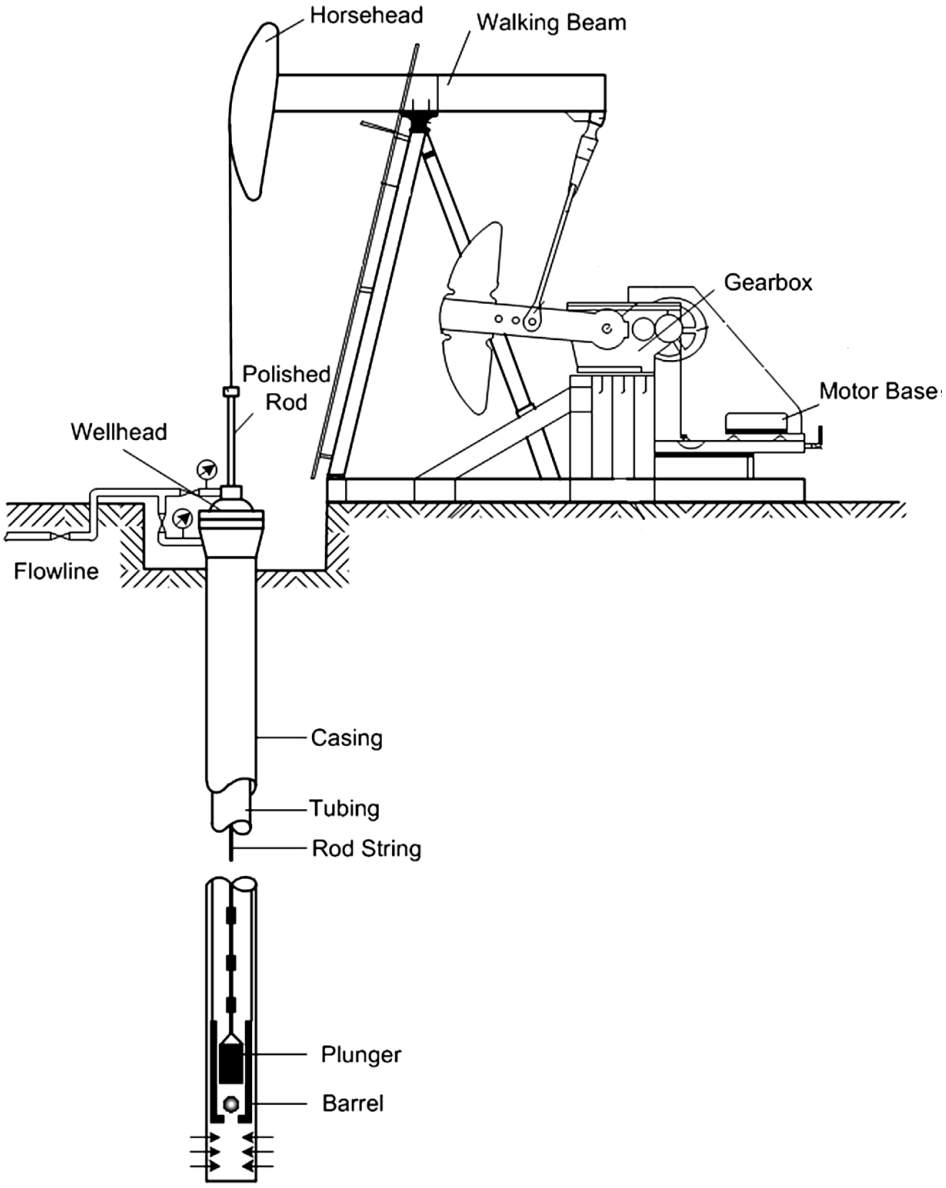

Figure 2.1: The components of a sucker-rod pumping system [2, p. 60]

2.1 Surface Equipment

The **prime mover** provides the driving power to the system and can be an electric motor or an internal combustion engine. The choice between the two is based on several factors like the power source availability, the horse-power requirement, efficiency, capital and operating costs. From this perspective, electrical motors are usually preferred. The most popular electrical motor in the oilfield is the one designated by the National Electrical Manufacturers Association (NEMA), NEMA D, which has the following advantageous features [2, pp. 237-239]:

- Highest breakaway torque among the NEMA series motors (275% of full load torque), facilitating easy starting of a pumping unit from a standstill;
- Peak output torque is close to the locked motor torque (breakaway torque);
- High slip (5–8%), which allows the reduction of gearbox torque and motor currents;
- Full load efficiency above 88%.

The Fig. 2.2 displays the typical qualitative performance curves of a NEMA D motor, as a function of motor speed, considering constant line voltage at the motor terminals. When the motor exceeds its synchronous speed (being driven by the well load), it behaves like a mechanical brake and an electrical generator simultaneously. In braking mode, depending on the control systems, the motor returns electrical power to the distribution system or generates heat. The efficiency curve variation highlights the importance of accurate sizing of the motors: oversized or undersized motors, running at a speed either too close or much lower than their synchronous speeds will have efficiencies much lower than if running at the rated speed.

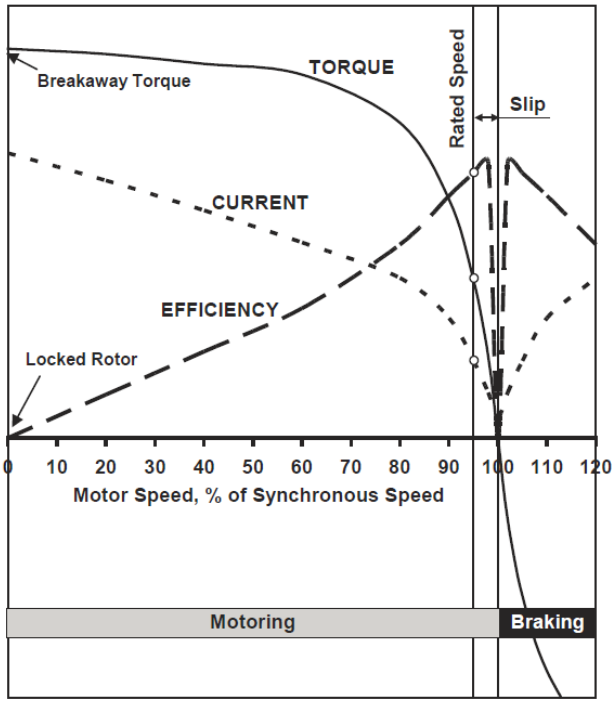

Figure 2.2: Qualitative performance curves for NEMA D electric motors [2, p. 239]

The **gear reducer** is indispensable to the pumping operation as it reduces the rotational speed of the prime mover to the pumping speed, and, inherently, increases the output torque to meet the well loads. The typical speed reduction ratio is 30 to 1, with a maximum output speed of about 20 SPM. Fig. 2.3 schematizes a typical geared reducer with double-reduction gearing. The high-speed shaft is driven by the prime mover and the low-speed shaft drives the pumping unit. A quiet and unsusceptible to failure operation is assured using herringbone tooth form, which provides uniform loading and resists torque reversals.

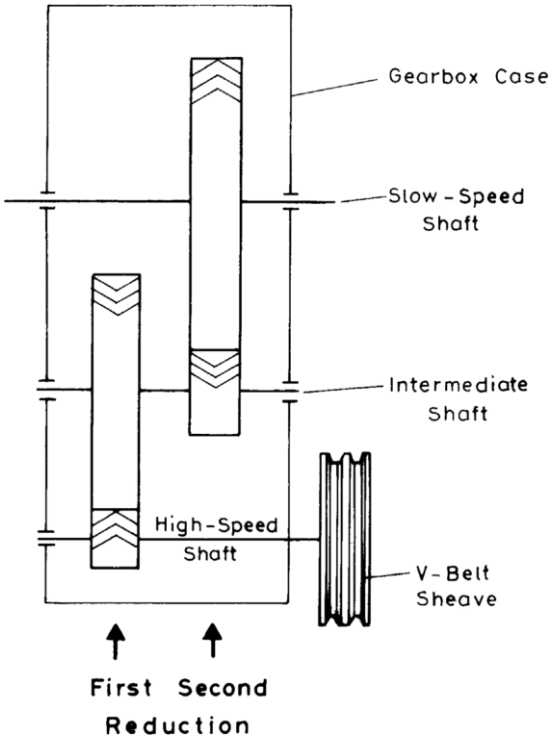

Figure 2.3: Schematic drawing of a double-reduction gear reducer [2, p. 227]

The **pumping unit** is the mechanical linkage that converts the rotations of the gear reducer into the reciprocating vertical movement output at the horse head. The sucker rods, attached to the horsehead, follow the movement and drive the downhole pump. Although there are many pumping unit geometries available, they all employ as a main element the walking beam, which works on the principle of a mechanical lever.

The Samson's post is the strongest and the most loaded member of the unit. It is the base of the saddle bearing which allows the walking beam to be pivoted. The well side of the walking beam is wreathed with the horsehead which conveys the vertical motion to the polished rod by means of the wireline hanger. In conventional units, the other side of the walking beam is connected to the crank arms by means of the equalizer and two pitmans. The crank arms have several wrist pins which allow the change of the stroke length of the unit. The counterweights are attached to the crank arms, and can be adjusted along the crank arm axis, to optimize unit loading.

The loading of the unit through the pumping cycle is highly irregular, peaking at the upstroke, while less to no power at all is needed at the downstroke (balancing of the unit plays here a

crucial role). Calculation of torque and power requirements throughout the cycle requires a careful evaluation of the pumping unit kinematic parameters.

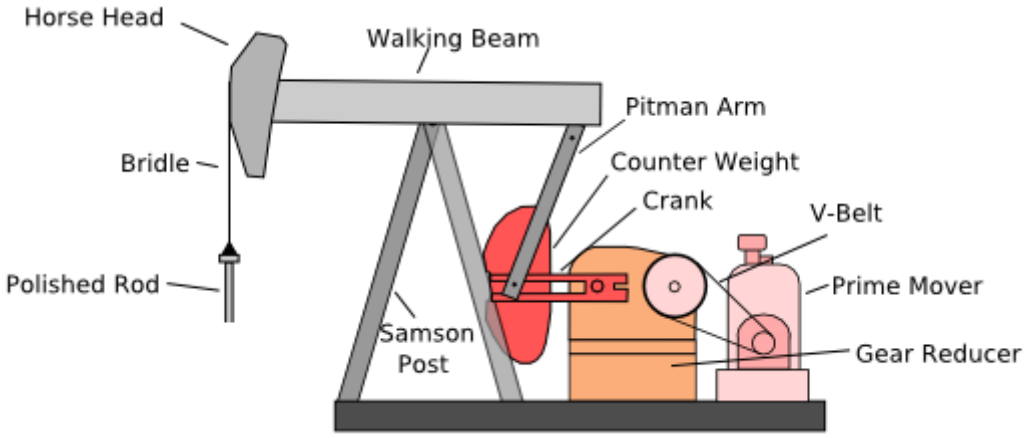

Figure 2.4: The structural parts of a common conventional pumping unit [8]

A typical **wellhead** arrangement of a sucker-rod pumping system is presented in the Fig. 2.5. The movement of the walking beam is transmitted to the polished rod through the carrier bar by the wireline hanger. The pumping tee installed on top of the tubing head deviates the produced fluids into the flowline, which also allows the flow of the gas accumulated in the casing. The stuffing box installed above the pumping tee prevents leaking of the well fluids into the atmosphere.

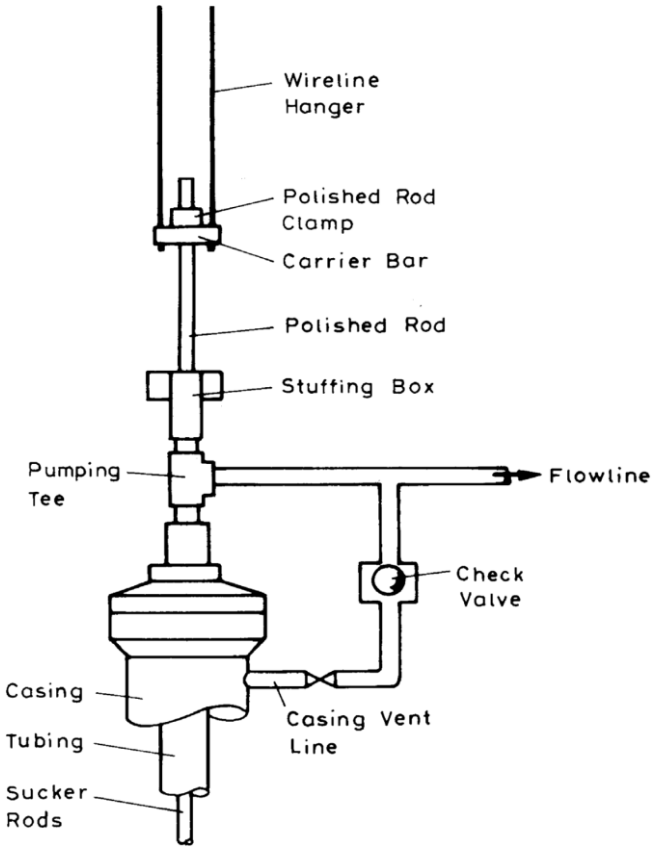

Figure 2.5: Wellhead arrangement of a typical sucker-rod pumping well [2, p. 195]

2.2 Downhole Equipment

The **downhole sucker-rod pump** operates on the positive displacement principle, and in fact, runs like any single acting piston pump. Its basic parts are the working barrel, the plunger and two ball valves which operate like check valves. Their opening and closing during the reciprocating movement of the plunger assures the displacement of the well fluids to the surface.

In the Fig. 2.6, which depicts a pumping cycle, after the plunger reaches its lowermost position, the traveling valve closes and the fluid above it is lifted towards the surface as the plunger begins its upward movement. The full load of the fluid column in the tubing string is carried by the plunger and the rod string connected to it, causing the string to stretch. During this interval, the inflow from the reservoir accumulates in the pump barrel, above the standing valve. During the downstroke, the traveling valve opens and the fluid load is shifted to the tubing, stretching it. As the plunger descends, the fluid from the barrel is transferred into the tubing. The operation of the valves can be seriously affected if optimum operating conditions are not sustained. This might imply either gas present in the pump barrel or incomplete pump filing.

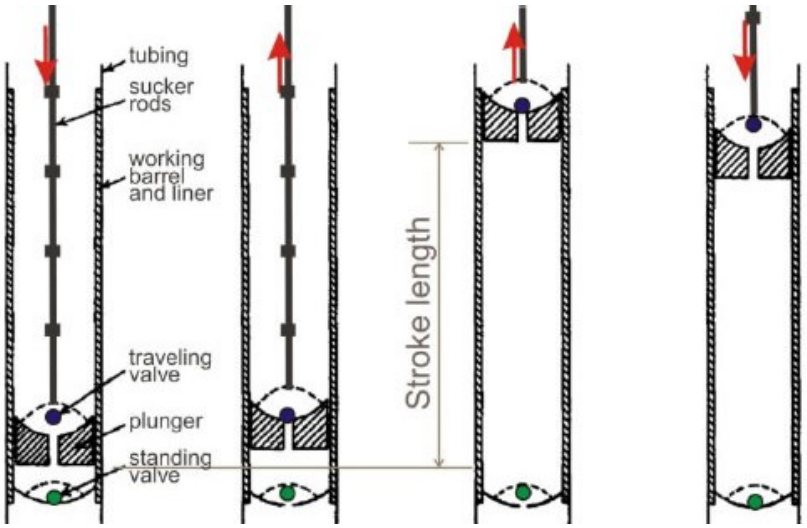

Figure 2.6: Schematic description of the pumping cycle [9, p. 12/163]

To limit the tubing stretching, which results in the reduction of the plunger stroke length, the tubing is being anchored, usually with an **anchor-catcher** (TAC) [2, p. 109]. This also limits the tubing helical buckling during the plunger upstroke [10, pp. 33-48]. Consequently, it reduces the tubing mechanical wear, reduces the loads on the pumping unit because of the reduced frictional forces between the rods and the tubing, thus reducing the torque and power needed for pumping.

In the case of a well with high GLR production, a vital component of the downhole equipment is the **gas separator**. It doesn't allow the free gas to enter the pump, therefore reducing its detrimental effects on downhole pumping:

- Decrease of the plunger's effective stroke due to delayed opening of the standing and traveling valve during the pumping cycle.
- Gas lock, which completely stops the pumping operation.

2.3 The Sucker-Rod String

The sucker rod string is the pivotal part of the sucker-rod pumping system, as it connects the downhole pump with the surface pumping unit.

2.3.1 Solid steel rods

Currently, the most widely used sucker rod type is the API standardized solid steel rod. They come in 25 or 30 feet length and rod body diameters from 1/5 to 1-¼ inch with 1/8 inch increments. Sucker-rods usually have pin ends which are hot forged and then machined and threaded. They are connected with short, 4 inch couplings with two box ends. These can be both full-sized or with a reduced outside diameter, designated for slim holes. The dimensional data of the rods and couplings is listed in the latest API Spec. 11B [11].

The elements of a sucker-rod pin end are presented in Fig. 2.7. where the short square section, called wrench flat, facilitates the use of power tongs for a proper makeup.

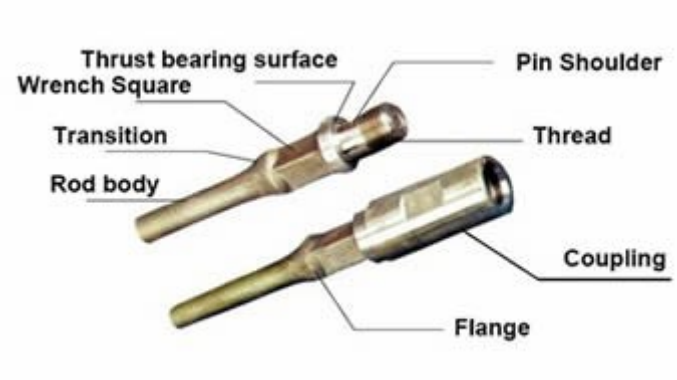

Figure 2.7: Construction details of a sucker-rod pin end [12]

The make-up of the pin-coupling connection has a critical effect on the integrity of the rod string. An improper tightening will determine a gradual unscrewing of the connection, ultimately resulting in the parting of the string. An increase in tightness will solve this issue, however, the material fatigue failure will become a much more likely problem. Due to their construction, the threads on both parts become stress raisers, which makes them highly susceptible to material fatigue, an effect enhanced by a corrosive environment or presence of the bending forces.

The classic API connection was first standardized in 1926 and hasn't been modified for a long time. In the past few decades, as the wells became deeper and crooked, the number of rod failures increased, establishing the joint as the weakest link in the system. Several improvements were applied in the attempt to reduce the causes of failures:

- the undercut thread, which is a slender neck on the pin with a diameter slightly smaller than the minor diameter of the threads, and acts as a stress reliever;
- Rolled threads, which eliminated the drawback of the cutting process, increased the strength of the thread-root and resulted in a higher surface finish quality of the threads, thus, reducing friction during make-up.

The standard API joint, however, still presents serious limitations of the thread design:

- Relative movement between the rod and coupling threads, heightened by high dynamic axial loads;
- The permanent deformation of the threads during makeup, which ultimately leads to microscopic cracks and fatigue failures;
- Non-uniform stress distribution, which overloads the first engaged threads.

Some of the alterations to the API rod and coupling design brought dramatical improvements to the rod load-carrying capacities, as is Carstensen's four-part connection system [13]. His design features a torque button squeezed between the pins and pre-stretching of the rod's neck to ensure a highly reliable connection. Fig 2.8 depicts the four-part arrangement.

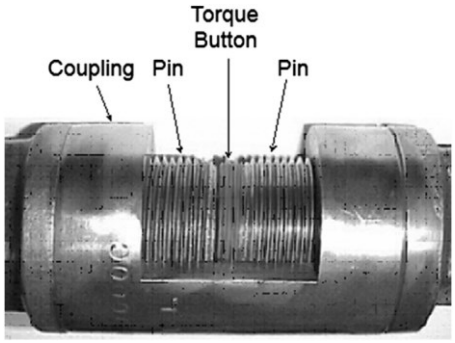

Figure 2.8: The four-part modified API connection [2, p. 133]

This construction results in reduced fatigue loading since both the pin and the coupling are highly pre-stressed, so the same tension stresses result in lower stress fluctuations and longer life. This arrangement is currently manufactured by Weatherford.

A completely new thread form was developed by Tenaris [14, pp. 26-29]. It features the following changes:

- Tapered pin and coupling threads with a trapezium profile;
- Flank-to-flank contact of the threads when engaged with diametrical interference;
- Low stresses in the rod pin after a proper makeup.

As seen on the Fig. 2.9, the stress distribution in the premium Tenaris joint is more uniform, and intrinsically eliminates the severe stress concentrations visible in the API connection. These connections, therefore, can withstand greater stress ranges and allow the production from deeper horizons and/or higher rates.

Figure 2.9: Comparison of the geometry and stress distribution in the API connection (left) versus a premium Tenaris connection (right) [14, p. 27]

Steel rods are normally made up form iron alloys, and subject to various treatments to increase their strength and hardness. The API rod grades materials and mechanical properties are described in the API Spec. 11B [11, p. 12]. By far, the most used material is the chrome-molybdenum alloy Grade D which allows for 115,000 psi tensile strength but has limitations regarding corrosive environments. Other grades available are Grade C, which are the cheapest one but resist only in non-corrosive environments and medium pumping depths, and Grade K, a nickel-molybdenum alloy, which has better resistance to corrosive elements, but lower tensile strength than Grade D.

Some special alloys and treatments allowed the increase of the rods' fatigue resistance and tensile strength. The high-tensile Weatherford EL are manufactured including a full-length induction hardening, resulting in a special binary construction of the rod material. Other non-API rods with very high tensile strength are Norris, LTV HS and Trico 66. Because of their very hard surfaces they are sensitive to handling and corrosion damage.

2.3.2 Continuous rods

As discussed earlier, the joints of the sucker-rod string are universally acknowledged to be the weak link of the system, inherently causing the majority of the downhole problems. A continuous string, without joints, therefore eliminates all the issues related to them.

The continuous rod technology was developed in early 1970's but was approached carefully due to special handling requirements and, therefore, high workover costs. Now, given the fact that their handling was facilitated by the means of inventions which ease the workover interventions, their popularity is rapidly increasing.

The original continuous rods, Corods [15], have a semi-elliptical cross-section, which allows the rod strings to be spooled onto special transport reels. A tapered rod string would be assembled (welded) prior to the rig operation and then run into the well via a special service rig. Due to the absence of connections, the lateral loads exerted by the string on the tubing are distributed uniformly, as illustrated in Fig. 2.10. The removal of couplings, centralizers and rod guides allows for a larger annular space and, therefore, minimizes pressure losses, increases system efficiency and reduces production costs. Moreover, due to their semi-elliptical shape, they have minimum two contact points with the production tubing in a given cross-section. Fig. 2.11 compares 1 inch slimhole sucker rods with 1 in (#6) Corods in a 2 3/8-inch tubing. Considering these effects, if similar side loads are assumed, reduced mechanical wear will result in substantially lengthened rod and tubing life.

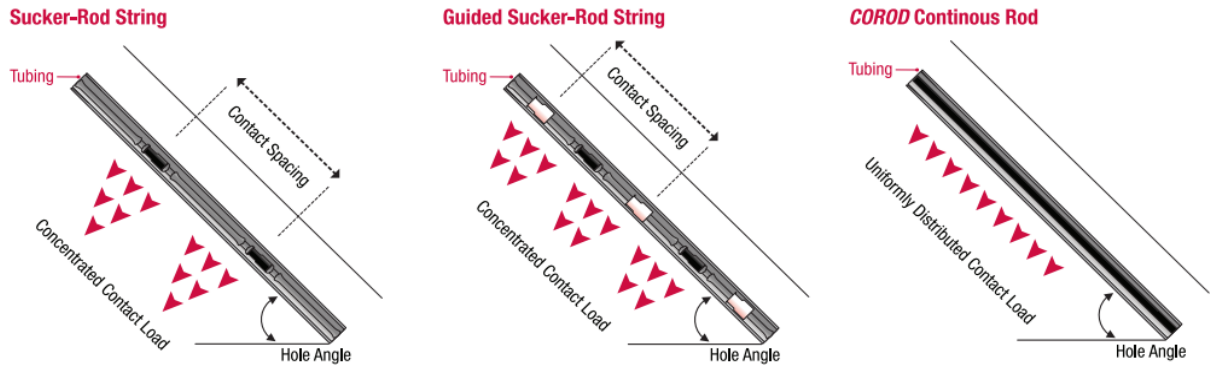

Figure 2.10: Comparison of the contact loads acting on the tubing [15, p. 3]

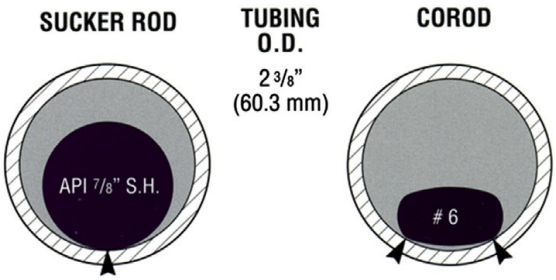

Figure 2.11: Comparison of rod-tubing contacts for coupled rods and Corods [2, p. 139]

Summing up the main advantages of continuous sucker rod application:

- Pumping speed can be increased because the risk of rod fall is eliminated;
- Slim hole advantageous: larger rod sizes may be used in the same size of tubing or a smaller tubing size may be used for the same rod size;
- Applicable to deviated boreholes: downhole friction between the tubing and the rod string is decreased because of the extended contact areas;
- Rod stresses and surface torque requirements are reduced allowing for larger volumes to be pumped.

A relatively new variation of Corods featuring a circular cross-section have been in use lately. They maintain the advantages of the original Corods but can be run in even smaller tubing sizes.

The nominal sizes of Corods is the outside diameter of a solid rod with the same cross-sectional area. They usually come in sizes from ¾ inch to 1-1/8 inch, with 1/16 increments and are made up from alloys with minimum tensile strength up to 145,000 psi (D special alloy) [15, p. 11].

The long-standing limitations of continuous rods, meaning the need for a special rig for well servicing and a special welding procedure for field repairs, are nowadays overcome by using a special injector head for coiled rod string and a portable, gas-fired butt-welding unit that can produce reliable welded connections in the oilfield [2, p. 140].

This type of rods is mainly used with insert pumps since it greatly reduces the time and cost of interventions (requiring a coil unit only), however, in case of the tubing pumps, the intervention costs will be significantly higher, requiring a workover rig as well as a coil unit.

2.3.3 Fiberglass sucker-rods

The use of glass-reinforced plastic, or fiberglass rods was first pioneered in 1970's as a mean to reduce corrosion related failures. Their light weight was later seen as solution to steel rods' overloading. This way, they become popular for overcoming two most problematic steel sucker-rod string drawbacks.

Fiberglass rods are made up from a plastic rod body with steel end fittings at the rods' ends (Fig. 2.12). The connector has standard API threads and has a special construction which allows for high gripping forces. The plastic body is a composite of thermosetting resin and of 1.5 million parallel, extremely thin glass fibers. Depending on the resin/glass ratio, the rods might have a tensile strength of 110-180,000 psi. This would make them about 25% stronger than steel rods, although weighing only one third of the steel rods with the same diameter. Due to their elastic behavior, they have an elongation of about four times of the steel rods. This fact limits their application to a combined sucker-rod string design featuring both fiberglass and steel rods. This allows an increase in string weight, especially in the bottom part which is often subject to compressive forces, but still weighs only a half of an all-steel string [2, pp. 140-142].

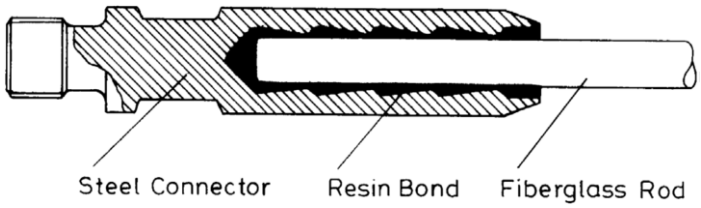

Figure 2.12: Schematics of an end connector for fiberglass sucker rods [2, p. 141]

The generally acknowledged benefits of using fiberglass sucker-rods in the string design are [16, pp. 58-59]:

- Reduced corrosion failures – applied in wells where numerous steel rod failures were attributed to corrosive conditions, the workover cost were dramatically reduced;
- Increased production – the highly elastic behavior of fiberglass sucker-rods can increment the pump plunger stroke with up to 50% of the surface stroke. This effect is enhanced if the pumping speed is near the string's resonant frequency.
- Reduced surface pumping system stresses – reduced weight of the string results in a great decrease of the torque rating and the structural capacity of the pumping unit under equivalent producing conditions. Or, the same amount of torque loading is used to lift higher fluid loads. The increased downhole stroke length allows the setting of a shorter surface stroke, which further reduces torque loading on the pumping unit.

- Decreased lifting costs – the reduction of string weight reduces energy required to run the pumping unit. The stretch of the fiberglass acts as stored energy, increasing system efficiency as well.

Their specific construction, however, has some limitations when applied to downhole pumping [2, p. 142]:

- Limited maximum temperature ratings – fiberglass rods shouldn't be used in designs where expected temperatures exceed those specified by manufacturers;
- Avoid compression loading – fiberglass has very low ratings for compression loading, therefore, their positioning within the string should avoid segments where buckling is expected;
- Careful handling – the relative softness of the material makes fiberglass rods susceptible to conception of weak spots if subject to undesired impacts;
- Investment costs – they are more expensive than steel rods, therefore, the rod-string design should be done properly if the justification of costs is desired.

3 Unified Model of the Pumping System

The cornerstone of a proper pumping system description is the simulation of rod string's behaviour. Due to its elasticity, the impulses generated by the motion of the pumping unit and the downhole pump are transformed into stress waves that travel along the string with the speed of sound. The interferences and reflections of these waves have a severe impact on the loads and displacements along the string.

Whilst the determination of polished rod load variation in time is a less pretentious exercise, the rod load variation at any cross section along the string is determined using the solution of wave equation as it is applied to rod pumping.

3.1 Rod Loads

Any eventual rod loads that can be encountered during a complete pumping cycle at any depth in the string can be classified into the following groups [2, pp. 143-144]:

- Rod weight: static axial load which, at any section in the rod string, is equal with the weight of the rods below the given section, peaking in the uppermost section of the string;
- Buoyancy force: static axial load equal to the hydraulic lift which is caused by the immersion of the rods in the produced liquid. It decreases the rod weight perceived at the surface. It is mostly perceived during the downstroke, and relatively negligible during the upstroke;
- Fluid load: static force that results from the hydrostatic pressure of the lifted fluid acting on the area of the pump plunger during the upstroke only;
- Dynamic loads: inertial forces and vibrations caused by changes in acceleration during the pumping cycle;
- Friction forces: sum of the fluid friction forces and mechanical friction between the rods and the tubing.

An analysis of these forces during a complete pumping cycle would show that the rod string is exposed to cyclic loading. Although the upper rod sections are constantly in tension, the magnitude of the resulting load is significantly higher during the upstroke. The static forces, in general, determine the range of load variation, however, with an increase of the pumping speed, the impact of the dynamic forces is more and more significant. The forces that excite the string at its two ends (at the surface through the polished rod, at the lower end by the subsurface pump) produce elastic force waves that travel in the rod material with the speed of the sound. These waves are of different magnitude and phase, and their interference and reflection can greatly affect the actual forces that occur in any rod section. Considering this, the sucker-rod string must be designed for fatigue endurance in order to withstand the pulsating tension it is facing.

3.1.1 Static loads

Static loads acting on the rod string are the result of a combination of the following forces: rod weight, fluid load, and buoyancy. Rod weight is constant for a defined sucker rod string. Fluid loads is supported by the sucker-rod string only during the upstroke, when the pump's traveling valve is closed. When it opens, during the downstroke, the fluid load is transferred to the tubing. This force acts at the bottom of the string and is always considered positive. Buoyancy, however, opposes previously mentioned forces, depends on the density of the fluid produced, and varies between up- and downstroke.

An advantageous way to determine the loads seen by the uppermost section of the sucker-rod string is define them according to the four basic phases of the pumping cycle [1, pp. 280-281]:

1. *Beginning of the upstroke – elastic deformation of the sucker-rod string while it picks up the fluid load*
   This phase is defined from the instant when the horsehead begins its movement upward, until the displacement, S_i, is equal to the total elongation of the sucker-rod string, λ. The equivalent crank rotation angle is φ_0. The crank position at a given moment is defined as:
   $$\varphi_i = i\frac{360^\circ}{n}\ ; \qquad i = 1,2,3,\dots,n;$$
   The resulting static force acting on the polished rod in this primary phase is:
   $$F_{ST,i} = \frac{S_i}{\lambda}(F_L + 2F_C) + \sum_{k=1}^{m} W_k\left(1-\frac{\rho_L}{\rho_S}\right)\left(1-\frac{A_{k-1}}{A_k}\right) - F_C \tag{3.1}$$
   Where $F_{ST,i}$ is the total static force acting on the polished rod in N, S_i is the displacement in m, λ is the sucker-rod string elongation in m, F_L is the fluid load in N, F_C is the Coulomb mechanical friction forces between the rods and the tubing in N, W is the weight of the rod string in air expressed in N and $\left(1-\frac{\rho_L}{\rho_S}\right)\left(1-\frac{A_{k-1}}{A_k}\right)$ is the buoyancy factor during the upstroke, considering that it acts only on the outstanding area of the connection between two rod sizes.
2. *Upstroke*
   From the moment the displacement of the polished rod equals the sucker-rod string elongation, the pump plunger begins its upstroke. The static loads will be constant until the end of the upstroke:
   $$F_{ST,i} = F_L + F_C + \sum_{k=1}^{m} W_k\left(1-\frac{\rho_L}{\rho_S}\right)\left(1-\frac{A_{k-1}}{A_k}\right) \tag{3.2}$$
3. *Beginning of the downstroke - elastic deformation of the sucker-rod string*
   Similar to the first phase, the relationship for the total static load is:
   $$F_{ST,i} = \frac{\lambda - S + S_i}{\lambda}(F_L + 2F_C) + W\left(1-\frac{\rho_L}{\rho_S}\right) - F_C \tag{3.3}$$
   where S is the surface stroke length, m.
4. *Downstroke*
   $$F_{ST,i} = W\left(1-\frac{\rho_L}{\rho_S}\right) - F_C \tag{3.4}$$

If only static forces are considered, a typical dynamometer card (variation of the polished rod load as a function of displacement) will be a parallelogram (Fig. 3.1).

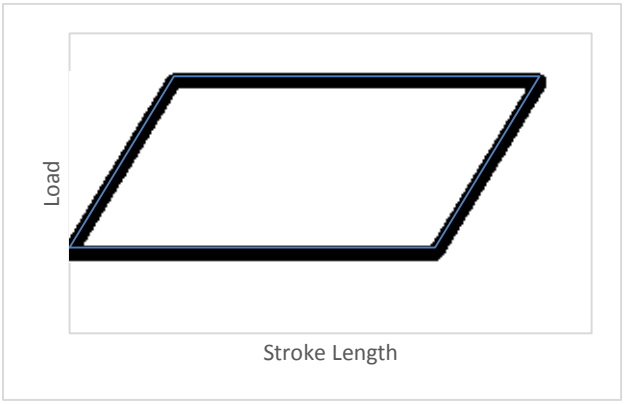

Figure 3.1: Hypothetical dynamometer card, if only the static loads were considered

3.1.2 Dynamic loads

Dynamic loads are generated by the inertial forces and vibrations in the sucker-rod string and the fluid column. They exist because of the sucker-rod string's speed variation, act in the direction of the speed change and are proportional to the rod mass. They are considered positive if they oppose the increase of the load at the polished rod, and negative if they oppose the decrease of the load at the polished rod.

The inertial forces during the upstroke should consider both the mass of the rods and the mass of the fluid column whilst during the downstroke only the mass of the rods is relevant. Due to the rod's elasticity, the horsehead movement is conveyed with a certain delay to the bottom of the string. Therefore, the acceleration of the transmitted movement will be different for different incremental rod elements.

The inertial force during the upstroke is [1, pp. 282-283]:

$$F_{in,i} = (F_L + W)\frac{a_i}{g}, \qquad i = 1,2,3,\dots,\frac{n}{2}, \tag{3.5}$$

Where $F_{in,i}$ is the inertial force in the string at the moment , in N, and a_i is the instantaneous acceleration at the moment i, in m/s^2.

The inertial force during the downstroke is:

$$F_{in,i} = W\frac{a_i}{g}, \qquad i = \frac{n}{2},\frac{n}{2}+1,\dots,n. \tag{3.6}$$

The normal operation of a sucker rod surface unit will generate vibrations which will spread through the sucker-rod string to the pump with a variable amplitude. Moreover, due to the pump's manner of operation (opening and closing valves, alternating support of the fluid load by the sucker-rod string and the tubing) additional free vibrations will be induced. Unlike static

forces, these vibrations have a maximum amplitude near the pump, and become attenuated up along the string.

3.2 The Wave Equation as applied to Rod Pumping

To understand and model the elastic behaviour of the rod string, oil industry uses the wave equation, which is derived from Newtonian dynamics and Hook's law of elasticity. It is ultimately used in the rod string design and prediction of the loads which the string will face during its lifetime. The derivation of this equation is given in many texts; however, Gibbs' version will be discussed here [17, pp. 34-39], since it also considers friction forces which play a major role in load modelling, especially if deviated boreholes are considered.

Fig. 3.2 depicts a rod string with a uniform cross-sectional area, A, and length, L. The x and u axes are the axial distance and displacement of the rod along the string, respectively, and increase downwards. The forces and velocities are also positive when oriented downward.

The forces acting on an incremental element of the rod are:

- W – the buoyant weight of the rod element;
- F_x – axial force representing the pull from above of the rod element;
- $F_{x+\Delta x}$ – axial force representing the downward pull of the rod element;
- F_d – a damping force which acts in the opposite direction of the rod movement, resulting from fluid and mechanical friction on the rod element's surface.

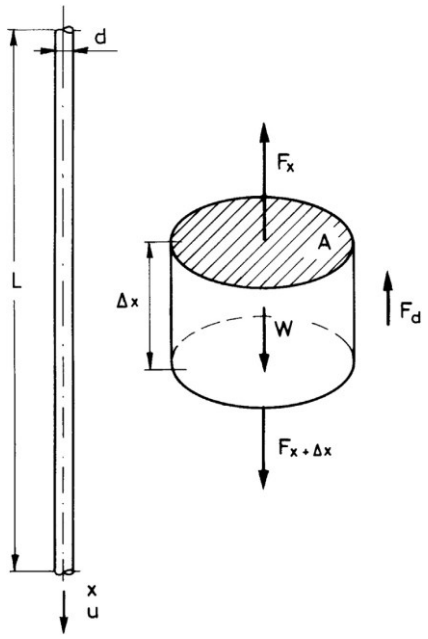

Figure 3.2: Forces acting on rod element [2, p. 275]

According to Newton's law, the mass of the rod times its acceleration should be equal to the force balance acting on the element. Considering the rod element relative to the fixed coordinate system of the well casing, the equation can be defined as [2, p. 274]:

$$\frac{\Delta x A \rho}{144 g_c}\frac{\partial^2 u}{\partial t^2} = EA\Delta x\frac{\partial^2 u}{\partial x^2} - F_d \tag{3.7}$$

In which weight is ignored as being a static force; the axial forces acting on the string are expressed as the actual deformation of the rod element according to the one-dimensional Hooke's law, E being the Young's modulus of elasticity of the rod material and $\frac{\partial u}{\partial x}$ - the rod strain, A is the cross-sectional area of the rod element, ρ is the density of the rod material and g_c and is the gravitational constant.

The role of the damping force in eq. 3.7 is to simulate energy removal from the string. In the borehole conditions, friction is a blend of fluid friction effects and Coulomb friction, which is rod-tubing drag. Fluid friction is a result of viscous forces arising in the annular space around the entire length of the rod string and is associated with the relative velocity between the rods and the fluid. Coulomb friction is not velocity dependent at all; it occurs at points where system components are in contact and depends on the normal force pushing the elements against each other and the friction factors involved. The net friction therefore cannot be described by a single formula since the different behavior of its two components.

In case of vertical or nearly-vertical wells, it is customary to approximate the sum of the damping forces with an equivalent viscous force, as is the Gibbs' approach [18]. In this case, the viscous damping force would be proportional to the shear velocity $\frac{\partial u}{\partial t}$ between the fluid and the rods. Gibbs' assumption also implies the damping force to be proportional to rod mass and is described by the following semi-empirical formula [2, p. 277]:

$$F_d = c\frac{\Delta x}{144}\frac{\rho A}{g_c}\frac{\partial u}{\partial t} \tag{3.8}$$

in which c is dependent on a damping factor, the sound velocity in the rod material and the total rod length [17, p. 36].

The conventional one-dimensional wave equation describing the propagation of force waves in the sucker-rod string can therefore be written as:

$$\frac{\rho A}{144 g_c}\frac{\partial^2 u}{\partial t^2} = EA\frac{\partial^2 u}{\partial x^2} - c\frac{\rho A}{144 g_c}\frac{\partial u}{\partial t} \tag{3.9}$$

The wave equation can be written in the form it is more familiar in rod pumping, in which the rod displacement u, is function of both the position, x, and the time, t:

$$\frac{\partial^2 u(x,t)}{\partial t^2} = v^2\frac{\partial^2 u(x,t)}{\partial x^2} - c\frac{\partial u(x,t)}{\partial t} \tag{3.10}$$

in which $u(x,t)$ is the rod displacement, c is the viscous dampening factor, $v = \sqrt{\frac{144 E g_c}{\rho}}$ – sound velocity in the rod material, x – position of the rods and t is the time.

It is a linear, second-order hyperbolic partial differential equation. This approach would introduce in the string design some theoretical shortcomings since it approximates the damping forces acting on the rod string. Yet, this friction law has been found to be useful and precise enough for practical purposes, at least in vertical wells.

In case of a deviated well trajectory, the wave equation should fulfill, in addition to proper handling of the fluid damping forces, a set of additional requirements:

- A gravity term must be considered to account for the variation of axial loads created by the interaction of rod weight and well inclination;
- Frictional Coulomb forces are substantial and should be considered as a cumulative of the following terms:
    - Friction forces in inclined straight sections as a function of rod weight;
    - Friction forces at doglegs that depend on the axial load present in the rods.

The modification of Gibbs' original one-dimensional equation features a 3D rod element, ds, and rod displacement, u, is a function of rod length measured along the well trajectory, s. The differential equation which includes the effects of well deviation is reproduced as follows [19]:

$$\frac{\partial^2 u(s,t)}{\partial t^2} = v^2 \frac{\partial^2 u(s,t)}{\partial s^2} - c\frac{\partial u(s,t)}{\partial t} - C(s) + g(s) \tag{3.11}$$

Where $u(s,t)$ is the rod displacement, c is the viscous damping factor, v_s is the sound velocity in the rod material, $C(s)$ is the term related to Coulomb friction, $g(s)$ is the term related to axial load from load weight, s is the rod length along the trajectory and t is the time.

The gravity term, $g(s)$, stands for the component of rod weight and is directly proportional to the inclination. The Coulomb friction term, $C(s)$, asks for the use of different formulas in straight and curved sections. The friction between the rods and the tubing surfaces is proportional to the normal force pressing the two surfaces against each other and the friction coefficient of the surfaces in contact (Fig. 3.3). In a dogleg, rod element, ds, is considered part of a circle with a radius dependent on the Dog Leg Severity (DLS). The side force is pointing to the center of the curvature, is related to the axial loads acting on the rod element and should also consider the selection of a proper friction coefficient.

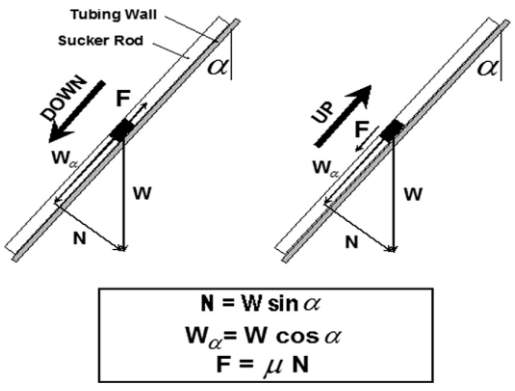

Figure 3.3: Rod weight and mechanical friction in a straight section of an inclined well [2, p. 301]

The solution of the damped wave equation allows the calculation of the rod displacement, u, at any axial distance, x, and any time, t. The main uses of this equation can be classified as:

- The diagnostic analysis, which calculates the displacements and forces along the string starting at the surface and proceeding downwards (seeks steady-state solutions only);
- The predictive analysis, which predicts the surface conditions based on the sucker rod pump's operation.

3.3 Unified Mathematical Model of the Pumping System

Although complex, the development of an accurate model to simulate the behavior of the sucker-rod system is essential. Predictions are useable and helpful as long as the assumption in the mathematical model closely mimic conditions found in the actual well. Once the predictions are proven to be trustworthy, the method is used to teach how rod-pumping equipment operates in the oilfield.

Starting from the prime mover and ending with the downhole pump, all the system's components interact with one another, integrating their specific behaviors into a unified system.

The prime mover's system performance can be plainly described by the output torque versus speed. After a prediction of motor speed throughout a complete pumping cycle is obtained, the torque-speed, current-speed and power-speed relationships can be derived and used in the integrated system model.

The mutual interactions between the prime mover, surface unit and the rod string is described using a crank-balanced unit. The equation integrating all the stated components can be written as [17, p. 362]:

$$I_t \frac{d^2\theta}{dt^2} = R_0 T_m - (T_{rod} - T_{cb} + T_{ai}) \tag{3.12}$$

Where I_t is the total rotary moment of inertia, θ is the crank angle, R_0 is the overall speed ratio, T_m is the prime-mover torque, T_{rod} is the rod-load torque, T_{cb} is the counterbalance torque and T_{ai} is the articulating inertia torque.

Rotary inertia effects arise from kinetic energy during the stroke. Kinetic energy is stored in the moving parts of the unit when instantaneous pumping speed increases, increasing the reducer's load. When the speed decreases, some of this energy will help the reducer decrease its instantaneous load. Articulating inertia effects are caused by changes in speed of the walking beam, horse head, equalizer beam assembly and pitmans. The reducer must therefore be able to provide additional energy to compensate these effects.

A further detailing of the equation's terms results in:

$$I_t \frac{d^2\theta}{dt^2} = R_0 T_m - f_t \left(E_1 A \frac{\partial y(0,t)}{\partial x} - U_s \right) + M_{cb} \sin(\theta + \tau) - \frac{f_t I_{ai}}{A} \frac{d^2\xi}{dt^2} \tag{3.13}$$

Where f_t is the torque factor, E_1 is the modulus of elasticity,A is the cross-sectional areas of the rods, $y(0,t)$ is the rod position relative to linear coordinate system, U_s is the structural unbalance, M_{cb} is the maximum counterbalance moment, τ is the counterbalance phase angle, I_{ai} is the moment of inertia of articulating elements and ξ is the beam angle.

This equation can only be solved using finite-difference equations, which give approximate but sufficiently accurate results. Each variable term is a function of crank angle θ:

- Prime-mover torque, T_m, depends on the motor speed which in its turn depends on the crank angle;
- Torque factor, f_t, depends on the crank angle for a given unit geometry;
- Rod position at the surface, $y(0,t)$, depends on the position of the carrier-bar which is a function of the crank angle;
- Beam angle, ξ, depends on crank angle and unit geometry.

Given these dependencies, a crank-angle function can be formed:

$$F(\theta) = R_0 T_m - f_t\left(E_1 A \frac{\partial y(0,t)}{\partial x} - U_s\right) + M_{cb}\sin(\theta+\tau) - \frac{f_t I_a}{A}\frac{d^2\xi}{dt^2} - I_t\frac{d^2\theta}{dt^2} \tag{3.14}$$

Replacing the derivatives with finite-difference quotients, it is possible to compute the zeroes of the function $F(\theta)$ using the Newton's method:

$$\theta_{j+1} = \theta_j - \frac{F(\theta_j)}{F'(\theta_j)} \tag{3.15}$$

In which j is the number of the iteration and $F'(\theta_j)$ is the derivative of the $F(\theta)$ function with respect to θ. The solution is reached when the difference $|\theta_{j+1} - \theta_j|$ is within the error margins.

The rod string is simulated using the wave equation as described in the previous section. In a predictive task, an exact solution cannot be reached, firstly because it is not possible to achieve an exact solution to the eq. 3.13, and secondly, because the subsurface pump boundary conditions cannot be stated before the beginning of calculations as it is dependent on the behavior of the sucker-rod string. This enforces the application of finite-difference approach to get a sense of the boundary conditions as the computed solution evolves.

The subsurface pump boundary condition cannot be precisely stated prior to beginning the solution. The times when pump valves open or close can be approximated only in course of solving the first iterations. The traveling valve closes at the moment the pump starts its upward stroke and would be characterized by a change from positive speed to a negative one (since the downward acting forces are considered positive). Therefore, considering the pump setting depth, L:

The plunger moves down while: $u(L,t) > u(L,t-\Delta t)$ (3.16)

The plunger moves up while: $u(L,t) < u(L,t-\Delta t)$ (3.17)

The plunger is not moving when: $u(L,t) = u(L,t-\Delta t)$ (3.18)

If the tubing is unanchored, the fluid load will transfer from the tubing to the rods when the traveling valve closes, causing the tubing to shorten. The total distance the pump moves relative to the fixed coordinate system (casing) in this case is:

$$S_t = \frac{F_f L_u}{E_t A_t} = \frac{F_f}{k_t} \tag{3.19}$$

In which F_f is the fluid load on the pump, k_t is the tubing stretch factor and L_u is the unanchored tubing length.

Considering the traveling valve closing time, t_{tvc}, the boundary condition defining the interaction between the rod string and the subsurface pump can be written as:

$$EA\frac{\partial u(L,t)}{\partial x} = k_t[u(L,t_{tvc}) - u(L,t)] \tag{3.20}$$

This boundary condition holds as long as condition stated in eq. 3.17 is true and:

$$0 \leq EA\frac{\partial u(L,t)}{\partial x} \leq F_f \tag{3.21}$$

When the tubing is anchored, the unanchored tubing length becomes negligible and the tubing stretch factor tends to infinite. To obtain a solution, the eq. 3.20 must be rewritten using a second-order finite-difference approximation to the derivative and solved for pump position at the time $t + \Delta t$:

$$u(L,t+\Delta t) = \frac{2k_t\Delta x u(L,t_{tvc}) + EA[4u(L-\Delta x,t+\Delta t) - u(L-2\Delta x,t+\Delta t)]}{3EA + 2k_t\Delta x} \tag{3.22}$$

At the time when the fluid load is fully transferred to the rods, and the standing valve opens, the boundary condition is changed to simulate a rising barrel with the fluid load acting on the bottom of the string:

$$F_f = EA\frac{\partial u(L,t)}{\partial x} \tag{3.23}$$

This boundary condition holds as long as condition stated in eq. 3.17 is true. When the plunger is at the top of its stroke, the standing valve closing time is reached, t_{svc}, and the fluid load is transferred back onto the tubing. The boundary conditions during this transfer will hold if the conditions stated in eq. 3.16 and eq. 3.21 are true.

When the load is fully released from the rods and the traveling valve opens:

$$EA\frac{\partial u(L,t)}{\partial x} = 0 \tag{3.24}$$

The downward movement of the rods with no fluid load applied is simulated by a finite-difference version of the eq. 3.24 as long as the condition stated in eq. 3.16 is true.

The ultimate object of simulating the pumping system is predicting the surface and subsurface pump dynamometer cards. These allow the system analysis, the prediction of extreme loads and stroke lengths, which eventually determine the system design featuring an optimal sucker-rod string.

Given the numerous amount of the stated approximations, a sucker rod string design based on the solution of the wave equation cannot be considered exact, but relatively thorough. It is the basis for the most recent string design methods, which claim to be accurate and integrated with the overall system design, therefore, providing a result which would closely mimic the real pumping conditions.

4 Sucker-Rod String Design Methods

One of the most vital components of Sucker Rod Pumping system optimization is the sucker rod string design. The performance of this piece of mechanical equipment, which due to its geometry behaves as a perfect slender bar, has an essential impact on the fluid lifting efficiency. Its failure will unquestionably lead to a total loss of production and have a negative impact on the key performance indicators (KPI). A properly designed rod string not only assures good operating conditions but can significantly reduce overall production costs as well.

During a complete pumping cycle, the sucker rod string is exposed to a combination of static and cyclic loads, as well as inertial forces, which must be considered in any design calculations to avoid failures and maximize system efficiency.

The main objectives of the rod string design are [2, p. 143]:

- The rod sizes;
- The optimum length of individual taper sections;
- The proper rod material.

The selection of the material for the sucker-rod string must consider the appropriate fatigue endurance limit that is the maximum stress level at which the equipment will operate under cyclic loading conditions for a minimum of 10 million complete cycles. This limit is primarily governed by the nature of loading (tension-compression, or more common for rod-strings, pulsating tension) and can be determined empirically. The presence of stress-raisers on the surface of the material also detrimentally affects the endurance limit, reducing rods' cross-section in time, and provoking fatigue failures. This outcome is even more secure in case of a harsh operating environment.

The fatigue endurance limits for steel structures have been long-established and used by means of the Goodman diagram which had to undergo several modifications to be useful in the sucker-rod string design:

- the maximum tensile stress should be less than the yield strength;
- compression must be avoided as it inevitably generates buckling and premature failure;
- harsh operating environments must be considered in calculations using a service factor.

This modified Goodman diagram is an industry standard as part of the API practices for calculation of allowable stress. The generalized formula, valid for different rod materials, emphasizes that the fatigue endurance limit varies with the minimum stress that occurs in the rod and the tensile strength of the steel material [20, p. 1]:

$$S_a = SF\left(\frac{T_a}{A} + BS_{min}\right) \tag{4.1}$$

Where S_a is the fatigue endurance limit (allowable stress) in psi, SF is the service factor, -, T_a is the minimum tensile strength of the rod material in psi, S_{min} is the minimum rod stress in psi, A and B are empirically determined constants, available for different steel grades as listed in Table 4.1.

Table 4.1: Material parameters used in the Goodman formula [20, p. 2]

Rod Type	T_a, **psi**	A	B
API Grade K	90000	4	0.5625
API Grade C	90000	4	0.5625
API Grade D	115000	4	0.5625
High-strength (HS)	140000	2.8	0.3750
Tenaris PC	125000	2.3	0.3750

When determining the allowable range of stress and allowable sucker rod stress for a string of sucker rods, API recommends the use of the modified Goodman stress diagram (Fig. 4.1).

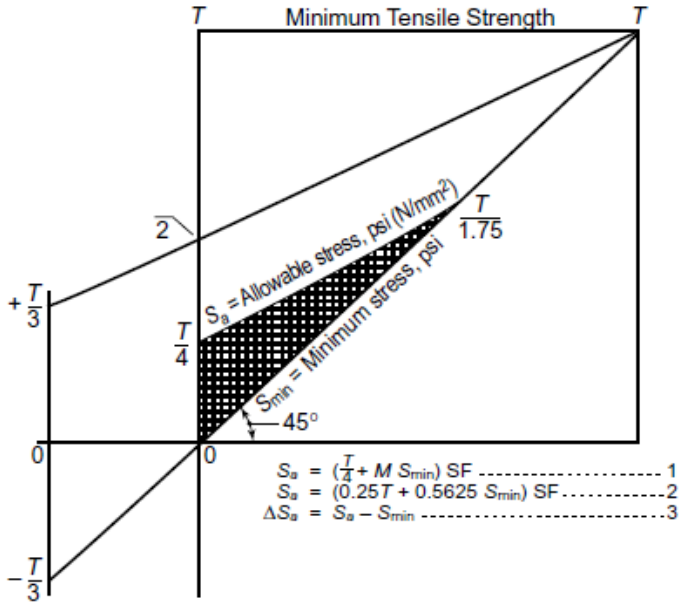

Figure 4.1: Modified Goodman diagram for allowable stress and range of stress for sucker rods in non-corrosive service [21, p. 3]

It provides the basic rating which can be used in non-corrosive media. But, since all well fluids are corrosive to some degree, the stress values determined from this diagram must be adjusted by an appropriate service factor, based on the severity of the corrosion and the

corrosion treatments used. In case of slimhole couplings, a derating factor must be included to account for reduced cross-sectional area.

The safe loading limits on the modified Goodman diagram are above the $S_{max} = 0$ line and below the S_a (allowable stress) line describing a given service factor. If maximum rod stress values, plotted against the appropriate minimum stresses, fall inside these limits, the rod string design is considered a safe one, allowing for failure-free continuous operation. Therefore, the aim of any string design method is to keep the stresses in the different taper sections within these safe operating limits [6, p. 3].

The non-API rods made from premium materials (Norris 97, Trico 66) have a wider allowable stress range because of their higher strength. Rods with premium Tenaris connections enlarge this range even more, exceeding the one of the rods made of grade D material (Fig. 4.2).

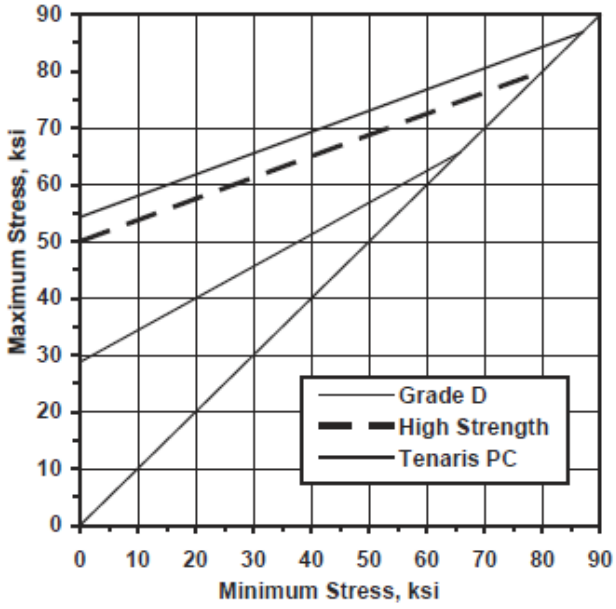

Figure 4.2: Comparison of the modified Goodman diagram valid for different rod materials [2, p. 159]

At the time of designing the rod loads cannot be entirely projected, partly because they also depend on the length and size of the tapers which are about to be calculated. Hence, some approximations need to be applied to find out the potential loads that will occur during pumping. From the early days of sucker-rod pumping till nowadays, due to the development of computing power, the assumptions and approximations used are closer to the real operating conditions in the well, mimicking the actual behavior of the string and resulting in designs which are sufficiently accurate. However, due to the multiple methods in use today, and the variety of wells with different trajectories, completions and working fluids, the choice of the optimal design model for a particular well remains a debatable issue.

4.1 Early simplified designs

The early rod string design methods all relied on the assumption that the sucker-rod string was subject to a simple tension loading [2, pp. 161-162]. The design principle was based on

keeping the rod stress at a value based on a percentage of the tensile strength of the rod material. One wide used method, adopted by API in early versions of RP 11L, was the one proposed in Bethlehem Sucker Rod Handbook [22]. It involves a design based on static loading by setting the maximum stress at the top of each taper equal, and then choosing the material which can handle this stress. The formulae are usually derived to determine the rod taper percentages.

This method gave reasonable results as long as it was used for vertical shallow wells, but became inadequate once the well designs progressed. Due to the obvious drawback of this design – its obliviousness to dynamic loads, the sucker rod strings would fail mainly because of fatigue of the rod joints subjected to cyclic loading.

This method is rarely used today, however, it might be considered when designing a sucker-rod string made of high-strength EL rods (Weatherford Electra high-strength rods). Because of the full-length induction hardening, the outer layer of the material is in extreme compression, up to 830 N/mm^2, value which is well above the usual tensile stresses imposed on the rod string. Material fatigue is mostly eliminated because the rod's surface is under compression during the complete pumping cycle and the range of stresses responsible for fatigue failures can be ignored. The maximum allowed stress in these rods is, therefore, a constant value, regardless of the range of stresses, as seen in the Fig. 4.3.

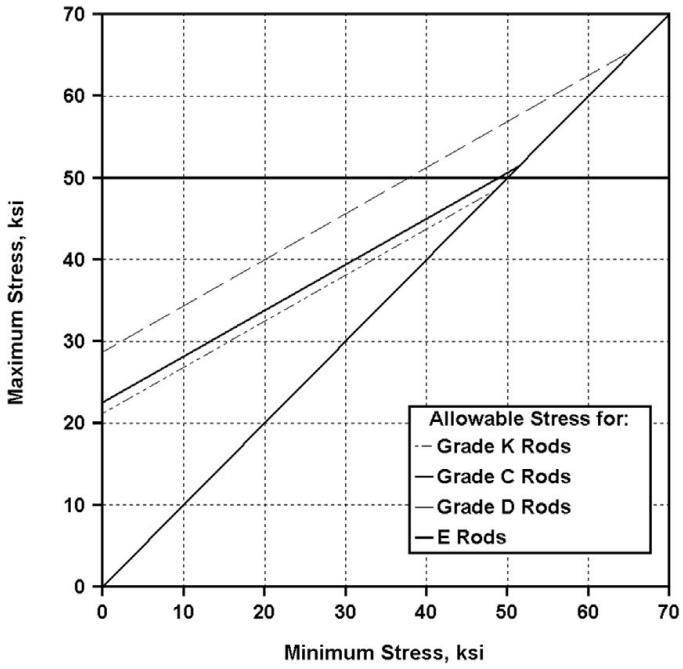

Figure 4.3: The modified Goodman diagram for various steel grades [2, p. 157]

Thus, this design method can be used successfully with this kind of rods, setting the peak stresses equal at the top of each rod section. Since the maximum allowable stress is considerably higher than the one of the API materials, fewer tapers with thinner rods are required resulting in the reduction of the string weight with all the associated advantages.

4.2 Designs considering dynamic loads

4.2.1 West's method

The first tapered rod string design procedure specifically developed for fatigue loading was proposed by West [3, pp. 68 - 77]. His design method attains to have the same ratio of maximum stress to allowable stress in each taper section, thus, the same safety factor for each taper. Rod strings designed in this manner will have the same safety factor included in every taper and will not have any weak points.

The maximum loads are calculated considering rod string weight in air, fluid load and a dynamic force calculated by means of the Mills acceleration factor method. It involves a simple harmonic motion of the sucker-rod string without considering fluid acceleration. In order to compensate for friction losses, West overlooks buoyancy effects, which tend to act in the opposite direction. These assumptions define a simplistic approach to the sucker-rod string design, nevertheless, results in reasonably predicted loads for small pumps and medium pumping depths.

For a single taper section, the minimum and maximum stresses are:

$$F_{min} = L\, w_r(2 - f) \tag{4.2}$$

$$F_{max} = F_0 + L\, w_r f \tag{4.3}$$

in which F_{min} and F_{max} are the minimum and maximum polished rod loads in lb, respectively, L is the length of the taper section in ft, w_r is the average weight of the taper section in lb/ft, F_0 is the fluid load on plunger in lb, S is the polished rod stroke length in in, N is the pumping speed in SPM and f is the Mills acceleration factor defined as:

$$f = \frac{2\pi^2 S N^2}{g} \tag{4.4}$$

The sucker-rod design implies an iterative procedure which follows the algorithm in the Fig. 4.4.

Assumption of the average rod string weight allows the calculation of the required ratio of maximum and allowable stresses, defined as follows:

$$R = \frac{F_0 + L_{total}\, w_{avg}\, f}{A_n \frac{Ta}{4} + 0.5625\, L_{total}\; w_{avg}\, (2-f)} \tag{4.5}$$

Where R is the ratio of maximum and allowable stresses, -, L_{total} is the total rod string length in ft, w_{avg} is the average rod string weight in lb/ft and A_n is the cross-sectional area of the top rod in in^2.

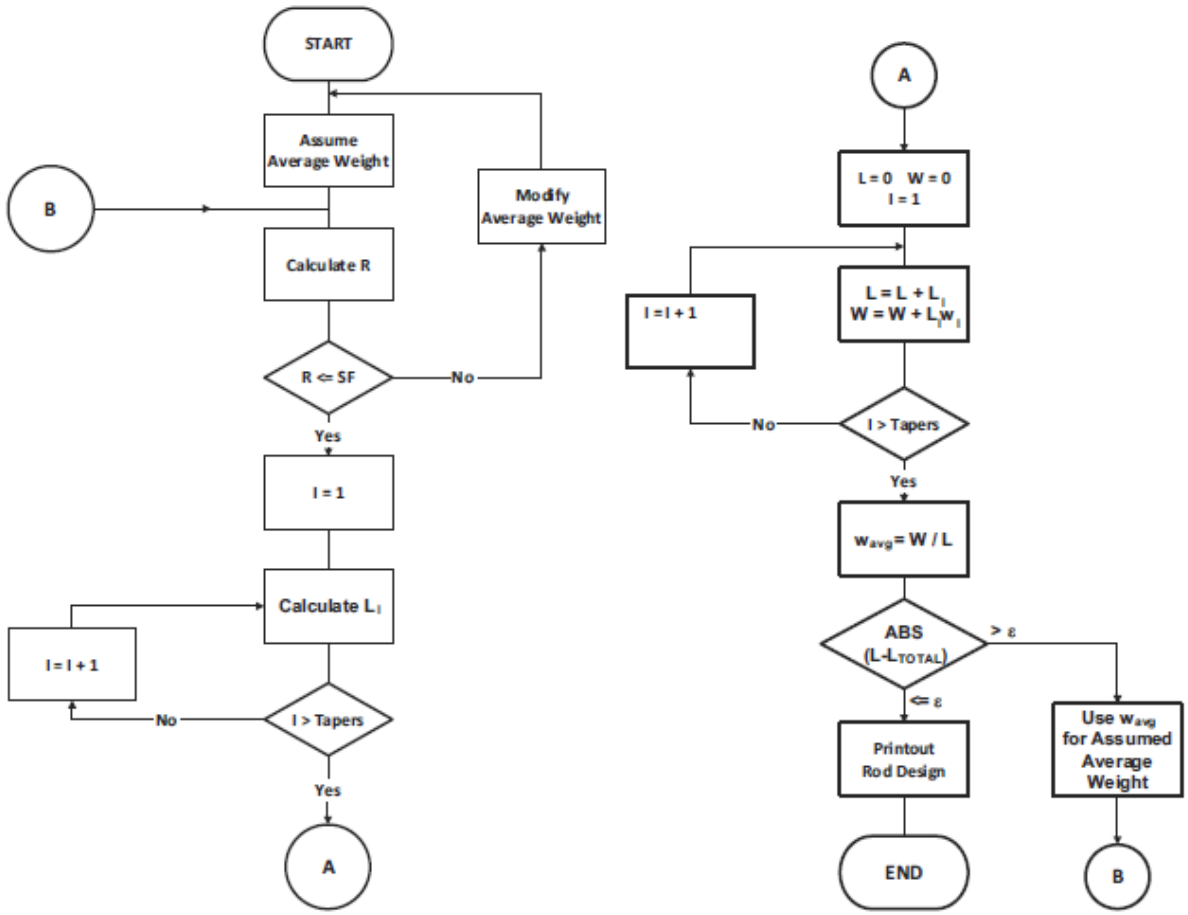

Figure 4.4: West's design procedure algorithm [2, p. 164]

The calculated value of R must be lower than the required service factor SF, otherwise the calculation must be repeated for another average string weight or a stronger material. The determination of a suitable ratio of maximum and allowable stresses allows the calculation of the taper lengths to fulfill the design requirements. An individual taper length is calculated as follows:

$$L_i = \frac{F_{\max(i-1)} - R\left[A_i \frac{Ta}{4} + 0.5626\, F_{\min(i-1)}\right]}{w_i\,[0.5625\, R(2-f) - f]} \tag{4.6}$$

L_i being the length of the i taper in ft, $F_{\max(i-1)}$ and $F_{\min(i-1)}$ being the maximum and minimum loads in the previous rod section in lb, A_i is the cross-sectional area of the i taper section in in^2 and w_i is the weight in air of the taper i in lb/ft.

In case the sum of the calculated taper lengths is different from the required pump setting depth, L_{total}, a new average rod value must be assumed, considering the calculated lengths, and the whole calculation must be repeated. The design procedure is complete when the convergence is found.

The utility of this method is limited by the accuracy of the Mills calculations and the manual iteration required for optimum taper lengths.

4.2.2 Neely's method

Later, Neely [4, pp. 58-66] introduced the design concept for equal "modified stress" at the top of each taper section. If a maximum and a minimum stress have been calculated or measured during a complete pumping cycle, the modified stress, S_{mod} in psi, is defined as the stress level that would give equivalent loading if the minimum stress during the pumping cycle was zero. It is calculated using the formula [6, p. 8]:

$$S_{mod} = S_{max} - 0.5625\, S_{min} \tag{4.7}$$

In case API steels are used, the attempt to keep the modified stresses equal would result in different service factors for different tapers. The $S_{mod} = constant$ line on the modified Goodman diagram, with a slope of 0.5625, will inevitably cross the equal service factor lines, which have a slope of $0.5625 \cdot SF$. Therefore, the sucker-rod string designed with this method will have higher service factors for the upper tapers, consequently, these will be more loaded than the lower ones.

The loads on the individual taper sections were calculated based on several simplifying assumptions. The dynamic load was calculated based on an empirical correlation, which was a function of pumping speed, fluid load, stroke length and used a simplified spring constant for the rod spring. The actual dynamic loads were calculated based on the following assumptions:

- Upstroke and downstroke dynamic forces are equal;
- Dynamic forces decrease linearly with string length, maximum at the surface and zero at the plunger.

This design procedure encountered for buoyancy but did not include rod friction, therefore, resulted in the taper designs which were not accurate enough.

4.2.3 API taper design

The American Petroleum Institute (API) adopted the rod string method proposed by Neely, including in later editions of RP 11L [5, pp. 8-10] the rod percentages calculated by this method, as a sole function of pump size. Consequently, a great number of sucker-rod strings were designed using this method, given the fact that it was easy and time saving, and gave reasonable outputs within some predetermined operating ranges.

The simplifying assumptions used by Neely, discussed in the previous section, in addition to some basic assumptions used for calculation of taper percentages in RP 11L, presented in the table 4.1, enforced serious limitations on the use of this design procedure [2, p. 168].

Table 4.2: Basic assumptions used for the calculation of taper percentages published in API RP 11L after Neely [2, p. 168]

Largest Rod Size, in	String Length, ft	Stroke Length, in	Pumping Speed, SPM
¾	4000	54	23.7
7/8	8000	120	11.6
1	8000	120	11.6
1 1/8	12000	192	8.8
1 ¼	12000	192	8.8

In case the operating conditions differ from the ones in the above table, the rod string based on the percentages listed in API RP 11L might significantly diverge from the optimum. As presented by Gault and Takacs in [6, pp. 5-8], for a 1-1/2 inch plunger and a rod string made up from 7/8 - ¾ inch rods, the rod percentages calculated with the API procedure do not vary with pumping conditions (pump depth and pumping speed), as they do if calculated with Neely's procedure (Fig. 4.5). Therefore, rod designs for operating conditions that differ from those assumed in the API RP 11L tables will unquestionably result in significantly different taper percentages. In this case, the use of the original Neely procedure is recommended.

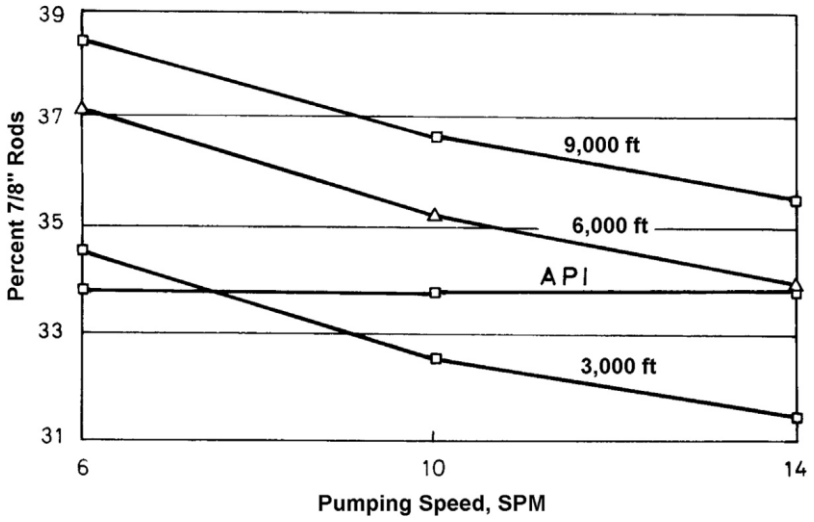

Figure 4.5: Comparison of API taper lengths with those calculated by Neely's method [2, p. 168]

The use of this shortcut method decreased in popularity as the computing power development permitted prioritization of accuracy against simplicity when it comes to sucker rod string design.

4.2.4 The Gault-Takacs method

A more theoretically thorough design method was developed by Gault and Takacs [6, pp. 4-8], which attempts to achieve the same degree of safety in every taper section, thus, a uniform level of fatigue loading all along the string. This would be the first method to consider the effects of force wave reflections that take place in the rod string in the load calculations. The dynamic loads are distributed along the string in proportion to the mass being moved and have different magnitudes during the up- and downstroke.

The polished rod loads, which reflect the sum of forces acting on the sucker-rod string, are calculated by the API RP 11L procedure [5, p. 5], which states the following formulas for the peak polished rod load, $PPRL$, and the minimum polished rod load, $MPRL$:

$$PPRL = W_{rf} + F_o + F_{du} \tag{4.8}$$

$$MPRL = W_{rf} - F_{dd} \tag{4.9}$$

Where W_{rf} is the buoyant rod string weight in lb and F_o is the fluid load on plunger in lb.

Knowing these, the dynamic load components on the upstroke, F_{du} in lb, and downstroke, F_{dd} in lb, can be expressed:

$$F_{du} = PPRL - W_{rf} - F_o \tag{4.10}$$

$$F_{dd} = W_{rf} - MPRL \tag{4.11}$$

Considering the distribution of the dynamic forces based on the mass being moving, the maximum, $F_{\max(i)}$, and minimum, $F_{\min(i)}$ in lb, loads at the top section of the taper i can be written as:

$$F_{\max(i)} = F_0 + \sum_{j=1}^{i} w_j L_j (1 - 0.128\gamma_L) + \frac{F_{du}}{W_r} \sum_{j=1}^{i} w_j L_j \tag{4.12}$$

$$F_{\min(i)} = \sum_{j=1}^{i} w_j L_j (1 - 0.128\gamma_L) - \frac{F_{dd}}{W_r} \sum_{j=1}^{i} w_j L_j \tag{4.13}$$

In which L_j is the length of the jth taper in ft, w_j is the average rod weight of the jth taper in lb/ft, γ_L is the specific gravity of the produced fluid and W_r is the total rod string weight in air in lb.

The rod stresses result:

$$S_{\max(i)} = \frac{1}{A_i}\left\{F_0 + \left[1 - 0.128\gamma_L + \frac{F_{du}}{W_r}\right] \sum_{j=1}^{i} w_j L_j\right\} \tag{4.14}$$

$$S_{\min(i)} = \frac{1}{A_i}\left\{\left[1 - 0.128\gamma_L - \frac{F_{dd}}{W_r}\right] \sum_{j=1}^{i} w_j L_j\right\} \tag{4.15}$$

$$S_{\max(i)} = \frac{F_o}{A_i} + S_{\min(i)} \frac{1 - 0.128\gamma_L + \frac{F_{du}}{W_r}}{1 - 0.128\gamma_L - \frac{F_{dd}}{W_r}} \tag{4.16}$$

where A_i is the cross-sectional area of the rods in the i[th] taper in in^2.

The Fig. 4.6 illustrates the step by step iterative procedure for the rod string design. Starting from assuming a rod material and arbitrary taper lengths, the peak and minimum polished rod loads can be calculated by means of the RP 11L formulas and used for further calculation of S_{max} and $S_{\min}$. Algorithm follows the calculation of an actual service factor for the top rod section:

$$SF_{act} = \frac{S_{max}}{\frac{T_a}{A} + BS_{min}} \tag{4.17}$$

Where SF_{act} is the actual service factor, S_{max} is the maximum stress in taper in psi, S_{min} is the minimum stress in taper in psi and T_a is the minimum tensile strength of rod material in psi.

This value becomes a starting point for the determination of the $SF = SF_{act}$ line equation. According to the design goal, the other taper strings must have the same service factor, thus, their $S_{max} - S_{min}$ points will lie on the same line. Simultaneously, these points must also satisfy the condition set in Eq. 4.16, consequently, satisfying the requirements of the design procedure.

The subsequent step in the design process is the determination of required minimum rod stresses, S_i^*, of the individual tapers:

$$S_i^* = \frac{SF_{act}\frac{T_a}{A} - \frac{F_o}{A_i}}{\frac{\frac{F_{du}}{W_r} + 1 - 0.128\gamma_L}{1 - 0.128\gamma_L - \frac{F_{dd}}{W_r} - BSF_{act}}} \tag{4.18}$$

These values must be used in the Eq. 4.15 to determine the minimum rod stresses as a function of rod length. Solving the equation for the i[th] taper length, the following final formula is derived:

$$L_i = \frac{1}{w_i}\left(\frac{A_i S_i^*}{1 - 0.128\gamma_L - \frac{F_{dd}}{W_r}} - \sum_{j=1}^{i-1} w_j L_j\right) \tag{4.19}$$

Afterwards, a check is made on their total length to match the pump setting depth. This results in an intermediate design, and usually the calculations must be repeated to achieve the optimum taper lengths which will satisfy the all the requirements. Moreover, the final SF_{act} must be checked, and in case it is higher than the current material's SF, a stronger material must be selected, and the calculations repeated.

It is an iterative procedure and requires more computational time but gives reasonably accurate results, and partly corrects the drawbacks and uncertainties inherently present in other string designs.

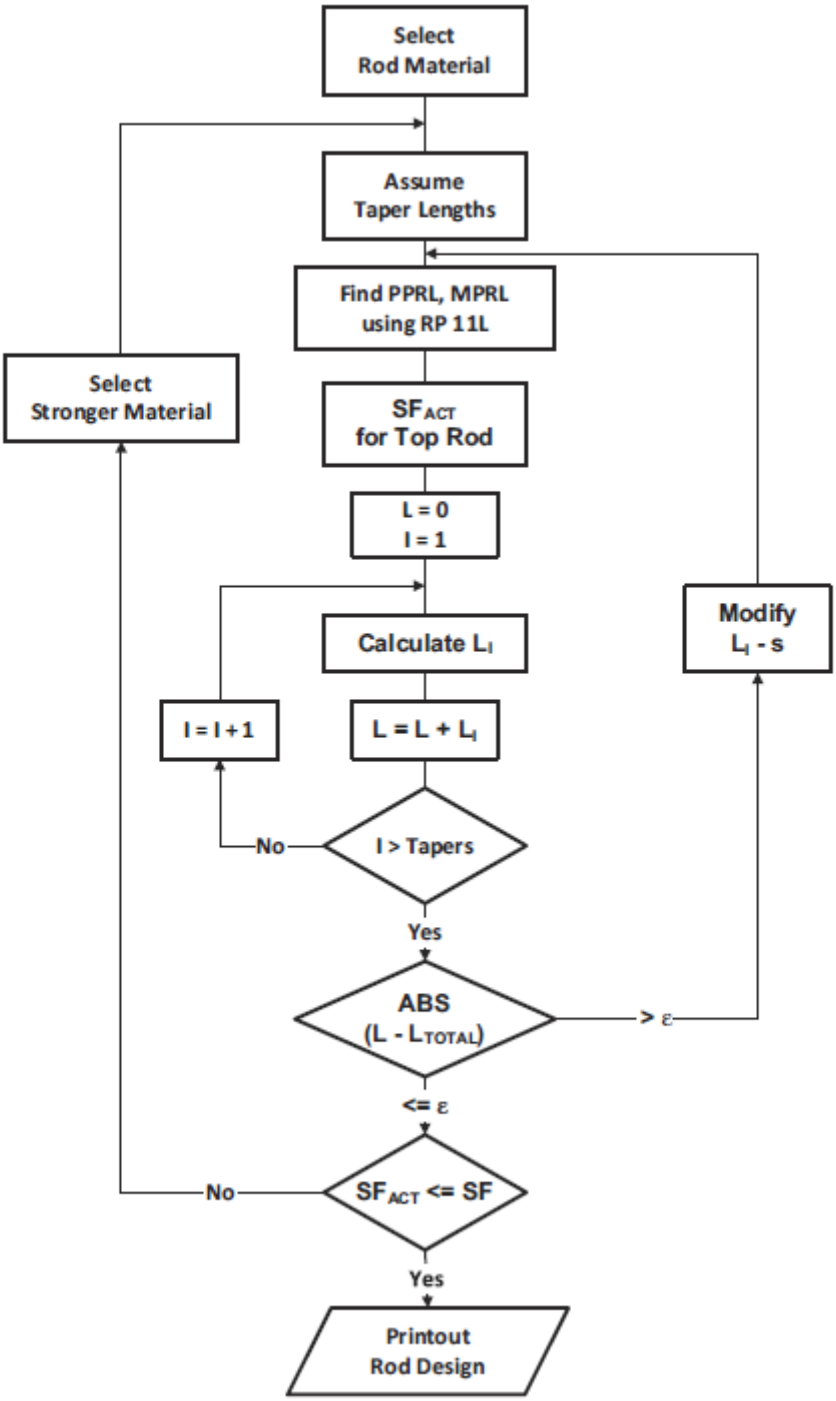

Figure 4.6: Algorithm for calculating rod string taper lengths with the Gault-Takacs method [2, p. 172]

4.2.5 Takacs – Gajda enhanced design model

As well as the previous design method, this enhanced rod string design procedure aims to select tapers that have the same level of safety against fatigue failure. However, as one of the main problems of a design method is the proper calculation of the rod loads during the pumping cycle, this method relies on calculation of rod loads from the solution of the 1D damped wave equation introduced by Gibbs. This way, the design procedure considers “true” mechanical

loads, and does not have to depend on many simplifying assumptions. However, the assumptions behind the solution of the 1D dampened wave equation must not be omitted.

As it is an iterative procedure, the starting point must be provided by a possible distribution of rod loads and stresses along a rod string.

They expressed the variation of minimum and maximum load in rod tapers as a function of taper length, l in ft, as follows:

$$F_{\max i} = a_i l + b_i \tag{4.20}$$

$$F_{\min i} = c_i l + d_i \tag{4.21}$$

Where $a_i \dots d_i$ are parameters of the best fitting lines representing rod load variation with depth.

The SF for the top of each taper can be expressed as the actual maximum load to the allowable load, or:

$$SF_i = \frac{F_{\max i}}{\frac{T}{A}A_i + BF_{\min i}} = \frac{a_i l + b_i}{\frac{T}{A}A_i + B(c_i l + d_i)} \tag{4.22}$$

This equation can be used to investigate the effect of changing the length of the taper for a fixed SF, if it is rewritten for the taper length, L_i:

$$L_i = \frac{SF\frac{T}{A}A_i + BSFd_i - b_i}{a_i - BSFc_i} \tag{4.23}$$

This equation embodies the cornerstone of this rod string design procedure, as it allows the calculation of the required length, L_i, of any taper based on the required or assumed SF value.

The calculation procedure for an arbitrary three-taper string would be following the next steps, referred to the Fig.4.7:

1. At the initial conditions (iteration $J = 0$), the taper lengths are calculated as equal parts from the total string length:
$$L_{1,0} = L_{2,0} = L_{3,0} = \frac{L_{total}}{3}$$
2. With the taper lengths being known, the predictive solution of the wave equation can be used to determine the distribution of the minimum and maximum loads along the entire length of the string. The minimum and maximum loads of the first taper are fitted with straight lines according to the Eq. 4.20 and 4.21, and the best fitting line parameters $a_1 \dots d_1$ are found.
3. The SF at the top of each taper is calculated with Eq. 4.22, and their average is determined, SF_0.
4. In the first iteration step ($J = 1$), the length of the bottom taper is modified as follows:

$$L_{1,1} = \frac{SF_0 \frac{T}{A} A_1 + B\, SF_0\, d_1 - b_1}{a_1 - B\, SF_0\, c_1} \tag{4.24}$$

$$L_{2,1} = L_{2,0} + \left(L_{1,0} - L_{1,1}\right) \tag{4.25}$$

$$L_{3,1} = L_{3,0}$$

5. The wave equation is solved for the modified taper lengths, and the distribution of minimum and maximum loads in taper 2 is used to find the parameters of the best fitting lines, $a_2 \ldots d_2$.

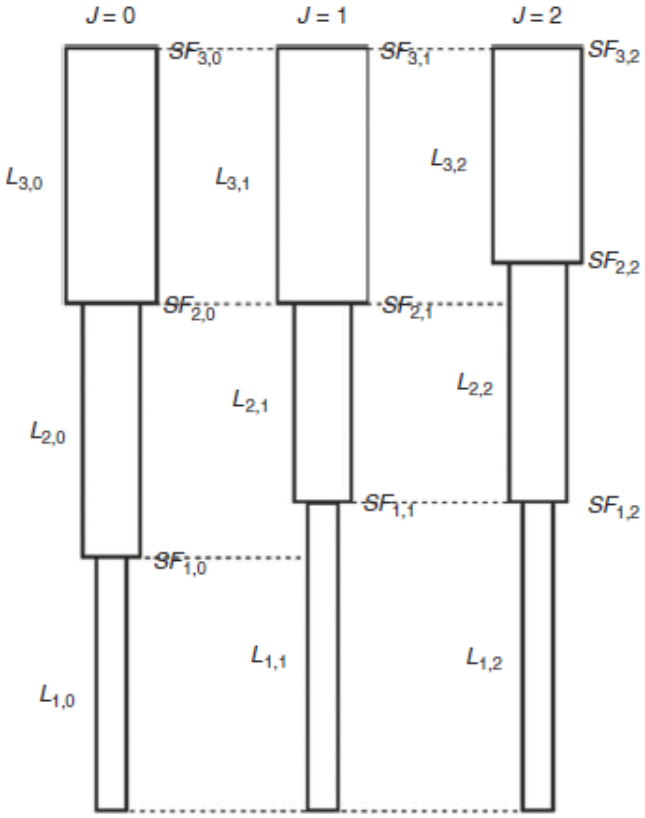

Figure 4.7: Illustration of the design procedure [20, p. 5]

6. The second iteration step ($J = 2$) starts with the adjustment of the length of the second taper:

$$L_{1,2} = L_{1,1}$$

$$L_{2,2} = \frac{SF_0 \frac{T}{A} A_2 + B\, SF_0\, d_2 - b_2}{a_2 - B\, SF_0\, c_2} \tag{4.26}$$

$$L_{3,2} = L_{total} - \sum_{i=1}^{2} L_{i,2} \tag{4.27}$$

7. The wave equation is solved again for the adjusted taper lengths. The SF at the top of each taper are calculated according to Eq. 4.22, and their average is determined, SF_2. The deviation of the individual SF values from the average is evaluated:

$$Error = \frac{\sum_{i=1}^{3}(SF_2 - SF_{i,2})^2}{3} \quad (4.28)$$

If the error falls between the admissible limits, the process has converged and the final string solution is reached. Otherwise, the string design from the second iteration must be further adjusted following the first iteration step procedure, and the entire process is repeated until the convergence is reached.

8. The converged SF is compared to the required one in a given field. If it is lower, the design is final, otherwise, the calculation must be repeated using different rod materials, number of tapers, or rod sizes.

Due to the fact that the prediction of rod loads is done based on the solution of the wave equation, this design can be considered as a much enhanced and accurate tool for the sucker-rod string design than the ones discussed previously, especially in vertical wells.

4.2.6 Method used in OMV Petrom

The method currently used in OMV Petrom is one based on the Virnovski's method from 1947, which was later modified by Grabovich and Kasyanov.

The method's base resides in the equivalence between the two asymmetric stress cycles if their mean stress is the same. Fig. 4.8 represents the fatigue endurance of a sucker-rod string (approximations made by Serensen and Kinasoshvili) in which the abscissa, σ_m, is the mean stress of a stress cycle, and the ordinate, σ_v is the variance of the stress from the mean. The σ_{-1} refers to the fatigue resistance in case of an alternative symmetrical stress cycle, σ_o in a pulsating stress cycle, σ_t is the tensile strength of the material and σ_y refers to the yield point of the material in static conditions.

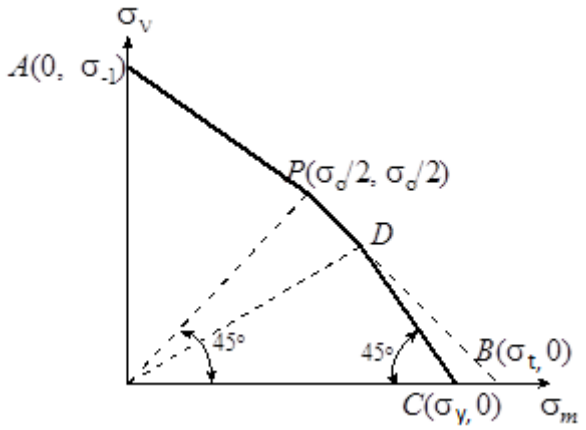

Figure 4.8: Serensen - Kinasoshvili diagram [1, p. 135]

In this diagram (Fig. 4.8), the operating range of a sucker-rod string is limited by the PDC line. The determination of the safety coefficient implies the application of the Soderberg criterion which says that two asymmetric stress cycles are similar when they have the same asymmetry coefficient, r:

$$r = \frac{\sigma_{min}}{\sigma_{max}} \tag{4.29}$$

In this case, Soderberg criterion would imply that the real stress cycle should have the same asymmetry factor as the limit stress cycle ($r = r_L$).

The safety coefficient is determined using the following equations in which the subscript L refers to the parameters of the limit stress cycle:

- PD line equation:

$$\sigma_{vL} = \frac{\sigma_o}{2\sigma_t - \sigma_o}(\sigma_t - \sigma_{mL}) \tag{4.30}$$

- Soderberg criterion ($r = r_L$):

$$r = \frac{\sigma_{min}}{\sigma_{max}} = \frac{\sigma_m - \sigma_v}{\sigma_m + \sigma_v} \tag{4.31}$$

$$r_L = \frac{\sigma_{minL}}{\sigma_{maxL}} = \frac{\sigma_{mL} - \sigma_{vL}}{\sigma_{mL} + \sigma_{vL}} \tag{4.32}$$

- Safety coefficient:

$$c_S = \frac{\sigma_{\max L}}{\sigma_{max}} = \frac{\sigma_{mL} + \sigma_{vL}}{\sigma_m + \sigma_v} \tag{4.33}$$

This method assumes that the safety coefficient should be equal at the top of each taper section and is recommended to be between 1,66 and 3:

$$c_{S_{i-1}} = c_{S_i} \ for\ i = 1 \dots n$$

The design procedure follows the next steps:

1. The upstroke and downstroke kinematic coefficients, m_{up} and m_{down} respectively, are calculated:

$$m_{up} = \frac{S\,n^2}{1790}\left(1 + \frac{R}{P}\right) \tag{4.34}$$

$$m_{down} = \frac{S\,n^2}{1790}\left(1 - \frac{R}{P}\right) \tag{4.35}$$

   In which S is the surface stroke length in m, n is the pumping speed in SPM, R is the crank shaft radius in m, and P is the pitman length in m.

2. To simplify the calculation, intermediate terms are derived:

$$A = L\left\{\left(b + f + m_{up}\right)(\sigma_t + \sigma_{-1}) - [b(1-f) - m_{down}](\sigma_t - \sigma_{-1})\right\}$$

   Where L is the pump setting depth in m, b is the buoyancy factor, f is the friction coefficient, σ_t is the tensile strength of the material in daN/cm^2 and σ_{-1} is the fatigue resistance in case of an alternative symmetrical stress cycle in daN/cm^2.

$$B = 10\,L\,\rho_L\,A\,(\sigma_t - \sigma_{-1}) \tag{4.36}$$

   In which ρ_L refers to the fluid density in kg/m^3 and A is the cross-sectional area of the rod in cm^2.

$$t = \frac{A + \frac{B}{q_{p1}}}{\frac{A_1}{w_1} + \frac{A_2 - A_1}{w_2} + \frac{A_3 - A_2}{w_3} + \frac{A_4 - A_3}{w_4}} \tag{4.37}$$

   In which w_i is the weight of the taper section in kg/m, and A_i is the cross-sectional area of the taper section in cm^2.

3. These will allow the determination of the taper lengths. For the first taper:

$$X_1 = \frac{t\,A_1 - B}{A\,w_1} \tag{4.38}$$

For the following tapers:

$$X_i = \frac{t\,(A_p - A_{i-1})}{A\,w_i} \tag{4.39}$$

4.2.7 The RodStar model

The commercial computer program package RodStar [7, pp. 60-68] incorporates the design of the rod string in the overall analysis of the rod-pumping system. This design procedure uses predicted rod loads that result from the solution of dampened wave equation. The taper lengths are determined iteratively so that their loading is identical at the top of each taper. Loading is defined as:

$$Loading = \frac{S_{\max 1} - S_{\min 1}}{S_{a1} - S_{\min 1}} = \frac{S_{\max 2} - S_{\min 2}}{S_{a2} - S_{\min 2}} = \frac{S_{\max 3} - S_{\min 3}}{S_{a3} - S_{\min 3}} = \cdots = C \tag{4.40}$$

Where $S_{\max i}$ and $S_{\min i}$ are the maximum and the minimum rod stresses in the ith taper in psi, S_{ai} is the allowed stress in the ith taper in psi, according to Eq. 4.1.

4.3 Design methods comparison

The main features of available rod string design procedure are presented in the Table 4.3.

Table 4.3: The main assumptions behind the Sucker-Rod String Design Methods

Model	Minimum Load	Maximum Load	Dynamic Loads	Design Goal
Bethlehem	-	Fluid load plus rod weight in air	-	Equal maximum stresses
West	Rod weight in air	Fluid load plus rod weight in air plus dynamic loads	Mills acceleration factor	SF = constant
Neely	Buoyant rod weight	Fluid load plus buoyant rod weight plus dynamic loads	Empiric formula	Equal modified stresses
Gault and Takacs	Buoyant rod weight	Fluid load plus buoyant rod weight plus dynamic loads	From *RP 11L*	SF = constant
Takacs and Gajda	Buoyant rod weight	Fluid load plus buoyant rod weight plus dynamic loads	From the solution of the 1D wave equation	SF = constant
OMV Petrom	Buoyant rod weight	Fluid load plus buoyant rod weight plus dynamic loads	Cinematic coefficients	c_s = constant

Investigation of the design goals of different models reveals huge differences in basic principles. The Bethlehem model results in string designs with the same maximum stresses at the top of each taper. When plotted on a modified Goodman diagram, the $S_{min} - S_{max}$ points for each taper section will fall on a horizontal line that must inevitably cross several $SF = constant$ lines. Lower tapers (with lower minimum stresses) have a higher service factor and lie closer to the allowed stress line. The fatigue loading on lower tapers is, therefore, higher, and these are more likely to experience premature failure.

Setting the service factors equal in each taper, as done by West (1973), Gault and Takacs (1990) and Takacs and Gajda (2014) ensures the same level of safety in every taper section and no weak points.

Neely's approach (1976) of setting the "modified stress" equal at the top of each taper, would mean that $S_{min} - S_{max}$ points belonging to the different tapers, plotted on the modified Goodman diagram, will lie on a line parallel to the $SF = 1$ line. This line, however, will cross the SF lines other than unity, meaning that this design will generate different safety factors for each taper, upper tapers being more loaded than the lower ones.

OMV Petrom's method relies on a non-sophisticated approach when it comes to the estimation of the dynamic loads, which, improved in time, has shown reasonably good results for the pool of wells currently in operation. Given that most of these wells have a non-crooked trajectory, low to medium pumping depths and relatively low fluid loads, the method has proven a viable and simple to operate algorithm for these specific conditions. However, when plotted on the modified Goodman diagram it proves to generate different service factors for each taper, therefore resulting in an unbalanced sucker rod string design.

The loads and stresses assumed in design procedures are built on the approximations of the actual pumping conditions. To have a precise evaluation of the sucker rod string design, one would have to physically measure the loads occurring in the designed strings. Since this is not a feasible approach, one would either have to rely on the calculation of the rod loads from the solution of the dampened wave equation written on the rod string, given the fact that the predictive solution of the equation results in loads that very closely match measurements, or, rely on a personalized approach for different types of operating conditions, defining limiting factors for the assumptions made behind the calculations.

Appendix A follows on the calculation results of the main design methods on two wells with different operating conditions. Well 1 is a medium depth well with low pumping speed and a large plunger diameter. Well two is a deeper well, with low pumping speed and smaller plunger diameter. These two wells define the average operating conditions for the region and are chosen as representative for the wells in OMV Petrom.

Design calculation results, along with plotted stresses on the Modified Goodman Diagram follow the general conclusions above, and provide a descriptive picture of the methods' differences. While RODSTAR method results in a design with relatively high service factors, which, though economical, might prove riskier, the OMV Petrom's method lies on the other

side of the spectra with conservative service factors, which could result in an oversized sucker rod string and higher initial expenses for the equipment.

The graphs illustrating the relative length, minimum and maximum stress can be used to check how accurate are the methods' stress calculations. For example, West's method taper lengths are fairly average in comparison with the other methods, but the minimum stresses of these tapers are largely higher than the average results given by other methods. Overestimation of the minimum stresses might lead to taper string design prone to buckling, therefore, this risk should be considered when using this design method. RODSTAR's results, on the other hand, tend to consider the widest range of rod stresses, having lower minimum stress results and higher maximum stress results compared to the rest of the methods. This might suggest good stress approximation, and consideration of a wider range of factors that can influence the rod stresses. OMV Petrom's method results trigger a much narrower range of stresses with significantly lower minimum and maximum stresses compared to the other methods, which might be caused by an underestimation of the forces acting on the string and an overall increased level of tensile rod failure.

4.4 Special rod type design particularities

As mentioned in the previous chapters, fiberglass rods are successfully used nowadays due to a range of advantages which allows cost reduction of the pumping operation. One of the advantages is the longer subsurface pump plunger stroke lengths relative to the polished rod strokes at the top of the string. This overtravel results from a dynamic amplification due to the fiberglass rod string operating near its first longitudinal natural frequency. If a rod string compound from heavy steel rods suspended below longitudinally elastic fiberglass rods is represented by a spring with an attached mass, as seen in the Fig. 4.9, then the natural frequency of a spring system is the frequency of free vibration of the mass when no external forces are present. Resonance occurs when the excitation frequency equals the natural frequency of the system, amplifying the displacement at the driven end of the spring. Forcing function corresponds here the polished rod-motion of the pumping unit. The sucker-rod system includes also the fluid load, which is not lifted on the downstroke, resulting in stretching of the rods on the upstroke to compensate for this additional load. Subsequently, the plunger stroke length is being reduced by an amount which is proportional to the fluid load.

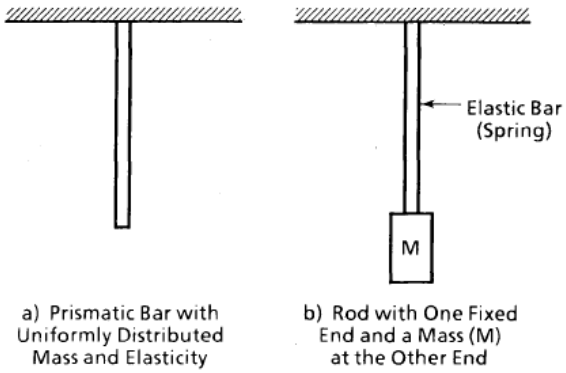

Figure 4.9: Mechanical models of sucker-rod strings [22, p. 347]

The rod-string natural frequency and rod stretch resulting from the fluid load are much more significant in fiberglass rod strings than in steel sucker-rod strings.

For a rod such as that shown in Fig. 4.8a, with the mass and elasticity uniformly distributed along its length, the first longitudinal natural frequency is expressed as [22, p. 346]:

$$\omega_n = \frac{\nu\,\pi}{2\,L_r} \tag{4.41}$$

Where ν –sound wave velocity (for steel $\nu = 16333\frac{ft}{s}$ or $\nu = 4978\frac{m}{s}$) and L_r – rod string length.

In strokes per minute, for a steel rood string, it can be expressed as:

$$N_o = \frac{245000}{L_r} \tag{4.42}$$

For all-steel rod strings, this natural frequency varies between 25 strokes/min for long strings and 80 strokes/min for shorter ones, which means that most steel sucker-rod strings operate at frequencies below 40% resonance, as shown in the Fig.4.9.

In case of fiberglass sucker-rod strings, most of the elasticity occurs in the fiberglass section, and 70 to 80% of the mass is concentrated in the steel rods at the bottom of the string. For a simple spring/mass system, with the spring containing a finite mass that is significantly smaller than the suspended mass, Tripp [22, p. 347] develops the following formulae:

$$\omega_n = \sqrt{\frac{k_t}{m_s + 0.3\,m_f}} \tag{4.43}$$

where

$$k_t = \frac{1}{\frac{1}{k_f} + \frac{1}{5\,k_s}} \tag{4.44}$$

In which k_f is the stiffness of the fiberglass section and k_s is the stiffness of the steel section, lbf-in (Nm).

Converted to strokes per minute:

$$N_o = \frac{60}{2\pi}\sqrt{\frac{k_t}{m_s + 0.3\,m_f}} \tag{4.45}$$

In Fig.4.10, the system response is presented as a function of non-dimensional parameters used in API RP 11L [5]. The abscissa is the ratio of pumping unit speed, N, to the rod-system natural frequency, N_o. The ordinate presents the ratio of the subsurface-pump plunger stroke, L_{dhp}, to the surface polished rod stroke, L_s.The relative stiffness of fiberglass sucker-rods is about one fifth the stiffness of the steel rods, which results in fiberglass-rod-string natural frequencies that are 50-60% of natural frequencies of steel rod-strings with the same lengths.

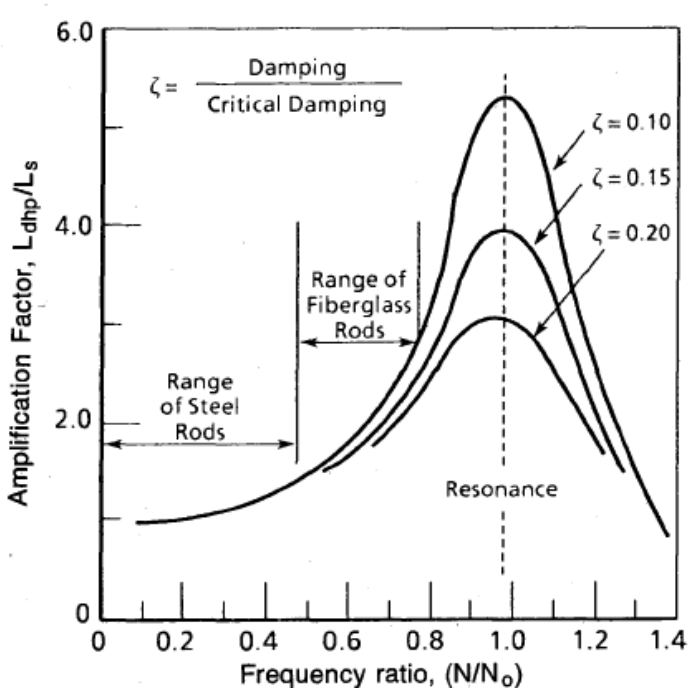

Figure 4.10: Effect of mechanical resonance on plunger stroke length [22, p. 348]

The forced-response curves show that, theoretically, fiberglass rod strings operating with $\frac{N}{N_o}$ values between 0,5 and 0,7 could have subsurface plunger strokes that are almost twice the subsurface polished rod-strokes. The fluid load lifted at the upstroke will reduce these strokes somewhat, but even so, many fiberglass rod strings will still operate with an amplification factor higher than unity.

The damping coefficient also has a considerable influence on the amplification factor in case the system operates with a frequency ratio of over 0,6.

To describe the fluid load influence on the rod stretch, API introduced another non-dimensional parameter, F_o/k, which relates the length of tubing stretch caused by the fluid load, $F_o/L_s k$, to the length of the surface polished rod stroke, L_s. When equal to 1, the entire polished rod stroke is used to stretch the rod, thus, no motion occurs at the plunger.

Due to their elasticity, relatively long or small diameter fiberglass rod sections of a rod string might limit production. As rod strings becomes more elastic, $F_o/L_s k$ increases, resulting in a shorter pump plunger length and less production. The effect of fluid load on subsurface plunger stroke length is shown in Fig 4.11, which highlights the reduction of plunger stroke length with the increase of the fluid load. As fluid load is also a direct function of pump diameter, maximum production can be achieved via compromise between the pump diameter, pumping speed and stroke length. For a given stroke length and rod string stiffness, a subsurface plunger diameter resulting in a $F_o/L_s k$ value between 0,45 and 0,65 was proved to result in maximum crude oil production [22, p. 349].

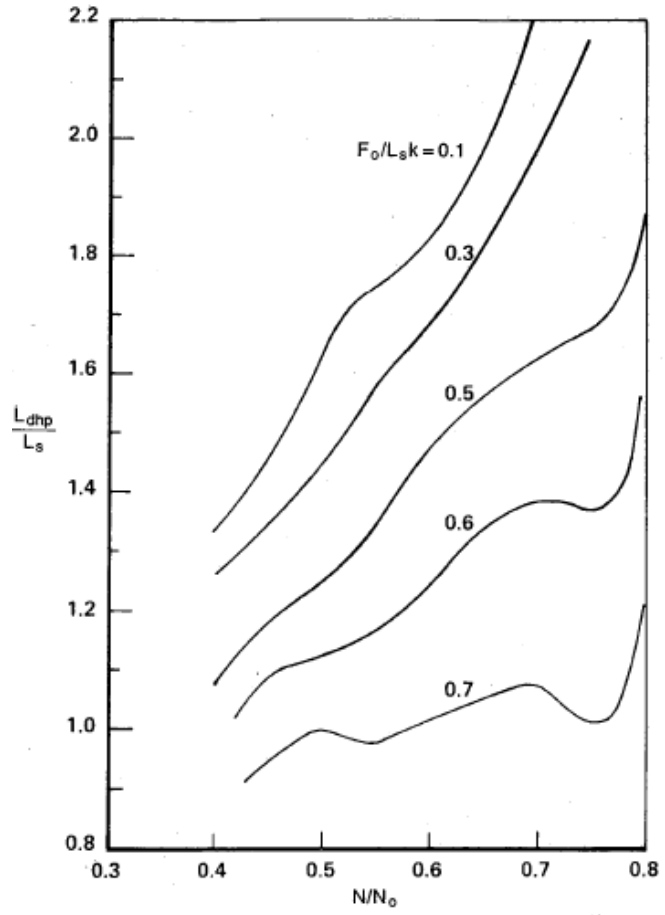

Figure 4.11: Pump stroke amplification as a function of speed and fluid load [22, p. 349]

Another design feature that must be accounted for when using fiberglass sucker-rod strings is the pump barrel and spacing design, which must account for longer subsurface stroke lengths than the polished rod stroke lengths, and consider the changes that will occur in time due to casing fluid level decrease (fluid load increase).

The design concepts and particularities for COROD strings is less different from the usual design, given that the material of which the string is made of is still steel. However, due to the lack of couplings, the fluid which would surround the joints and add to the effective moving mass is taken out of the equation, resulting in diminution of the dynamic loads.

5 Rod String Failures

The sucker-rod pumping system failures happen mostly due to the failures of one of the three main components: the subsurface pump, the sucker-rod string and the tubing. Failure of one of these components intrinsically implies non-productive time and additional costs, therefore, inspection of the main causes of break down are vital to a better system design and reduction of failure frequency.

The sucker-rod string's main function is to convey the reciprocating movement from the pumping unit to the piston of the subsurface pump. Due to severe working environments, alternative loading, well path deviation, impurities in the produced media, this part of the system is susceptible to failures, as seen in Fig. 5.1, which directly affects the production costs.

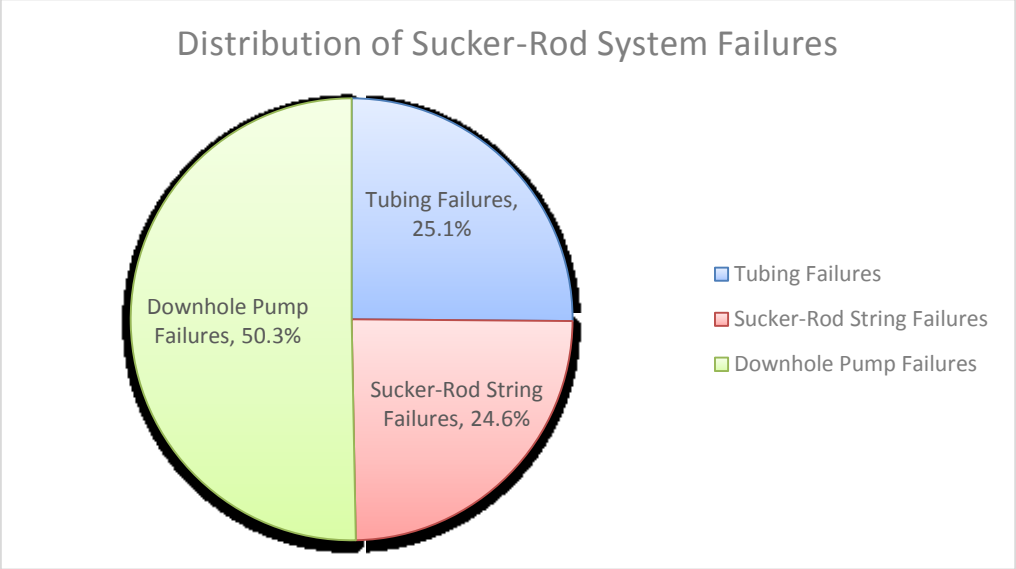

Figure 5.1: Distribution of Sucker-Rod String System failures in OMV Petrom for 2016

5.1 Types of failure

Generally, sucker-rod string failures can be distinguished as tensile or fatigue failures. Tensile failures are rare and happen because the material's tensile strength is exceeded. They are easily identified by the permanent stretch of the rod at the point of failure and by the coarse, granular break faces, as seen in the Fig. 5.1. These types of failure can be avoided by properly designing the rod string. The majority of rod-string failures are fatigue-type breaks. They start at the surface of the rod at some stress raiser (nick, dent, crack) which reduces the metal cross-section and causes an overload due to the stress concentration. The initial crack progresses at right angles to the stress as the material cross-section is further reduced. After a number of load reversals, the remaining metal area can no longer support the load and fails in a tensile break. The fatigue break face is divided into a smooth, polished, crescent-shape pattern and a coarse, granular break surface, typical for tensile breaks (Fig. 5.2).

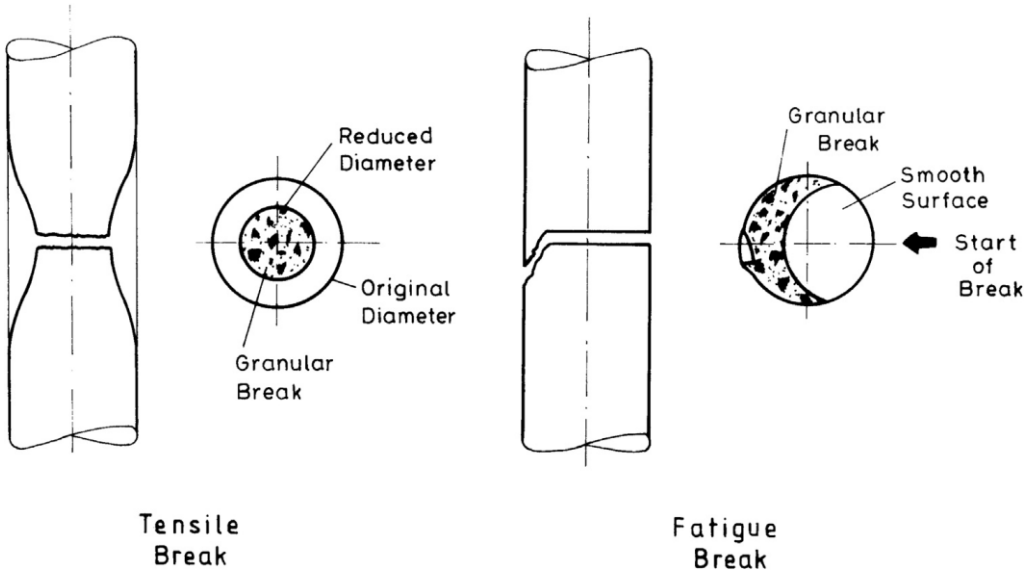

Figure 5.2: Typical tensile and fatigue failures of a sucker rod body [2, p. 179]

The primary consideration for preventing the rod failures are therefore:

- Keeping the stresses within safe limits of the modified Goodman diagram;
- Reducing the number and severity of the stress raisers by proper handling;
- Inhibiting corrosion.

5.1.1 Rod Body Failures

Breaks in the rod body are almost exclusively fatigue failures caused by mechanical or corrosive damages, or a combination of both.

Most mechanical damages occur on the surface of the rods as nicks or dents caused by tools or other steel parts. In deviated wells, or unanchored tubing, rod body wear can be excessive and contribute to rod failures. Bent or corkscrewed sucker-rods will inevitably fail if subject to tensional loads, due to an overload on the concave side of the bend. Therefore, the rods must be checked for straightness prior to running in the well, and discarded in case they are bent. Rod flexing is also a common cause of mechanical damage, as lateral movement of the rods results in local stresses at the point where the movement is transmitted by the rigid joint to a more flexible body. Lateral movements can be generated by shock waves as the ones generated in a fluid pond scenario. Failure closer to the joint can also be caused by the pin offset from the rod axis, as a result of manufacturing error.

Corrosion damage works on a chemical or electrochemical principle and removes part of the metal from the surface of the rod. In lightly loaded strings, corrosion damage leads to an eventual tensile break, due to continuous reduction of the metal cross-section. In deeper and heavier-loaded wells, corrosion damage acts as stress concentrator, ultimately leading to stress corrosion fatigue failure. Reduction of corrosion related problems can be achieved with a proper corrosion inhibition program, specific to the corrosive environment present in the particular well (sweet, sour, galvanic, bacteria).

5.1.2 Joint failures

Joint failures occur mostly because the contact between the pin shoulder face and the coupling face is lost. An improper make-up, whether too tight or too loose, will inevitably lead to a fatigue failure, either of the pin or the coupling. When joint tightness is lost under the pumping load, the pin starts to move laterally inside the coupling. While the threaded section of the pin is held rigid by the coupling threads, the undercut section is periodically bent with the vibrations in the rod string causing a small fatigue crack to appear at the root of one of the threads. The small crack slowly progresses into the metal area, and the pin will break when the remaining metal area is insufficient to carry the well load. Pin breaks can occur at various places in the pin, depending on the grade of looseness in the joint.

Coupling breaks are mainly attributed to the loss of tightness in the sucker-rod joint and the bending forces associated with it. The failure starts at a stress raiser and grows at right angles to the axis of the coupling, resulting in a characteristic fatigue-type break face.

Overtightening of the joint can damage the couplings in case if, during makeup, too much torque is applied, the yield strength of the material is reached, resulting in permanent deformation. The outside diameter of the coupling increases, the coupling flares out, and it can even split at the ends. This is tensile-type damage and always occurs at the two ends of the coupling.

An improper make-up can result even in the total unscrewing of the joints, if aided by tangential stresses in the rod-string and vibrations.

5.2 Failure statistics within OMV Petrom

According to the database of well interventions within 2016, the main causes the sucker-rod string failed or were replaced are frictional wear due to contact with the tubing, as well as normal wear due to being in continuous contact with circulating fluid and the impurities it contains, and material fatigue (Fig. 5.3).

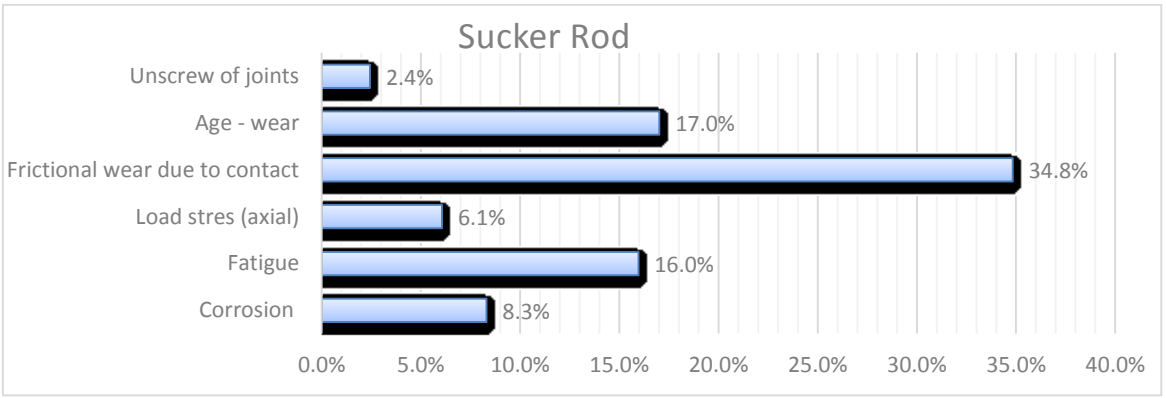

Figure 5.3: Sucker-Rod String failure reasons within the OMV Petrom in 2016

Frictional wear can be caused by an unsuccessful design of the rod string, which does not account for buckling, causing the string to bend and touch the tubing, as well as inflict alternating stress on the rod material which could aid fatigue failures.

Fig. 5.4 depicts the distribution of the sucker-rod string replacement interventions based on the parts that were the weaklings. It is easily noticed that in most of the cases, the sucker-rod joint is the main part that fails, therefore, for an ultimate increase in the meantime between failures (MTBF), addressing this issue is crucial.

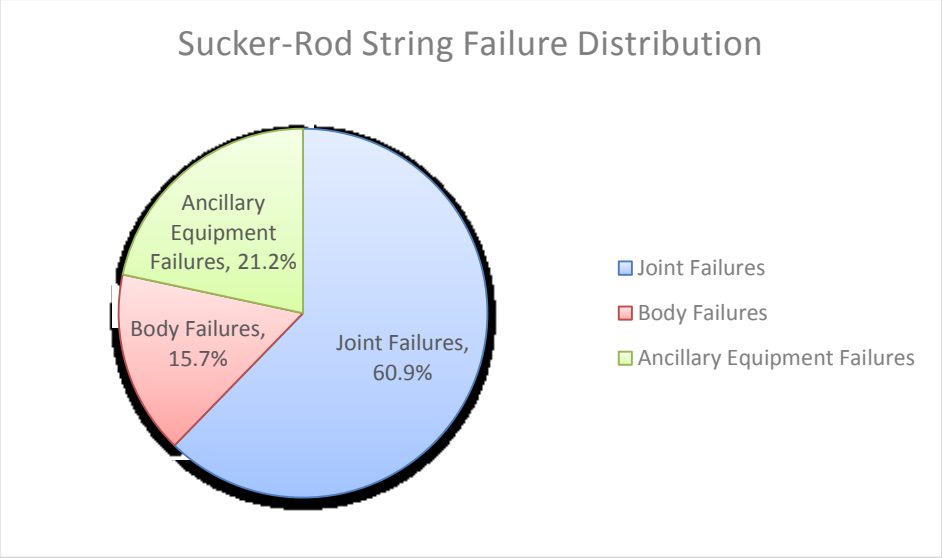

Figure 5.4: Distribution of Sucker-Rod String Failures within OMV Petrom in 2016

As illustrated in the Fig. 5.5, the connections mostly fail because of the frictional wear, as, due to their larger diameter, they act as support points if there are any induced lateral forces in the string. Fatigue is also a common cause of failure and is responsible for nearly 20% of the rod connection failures.

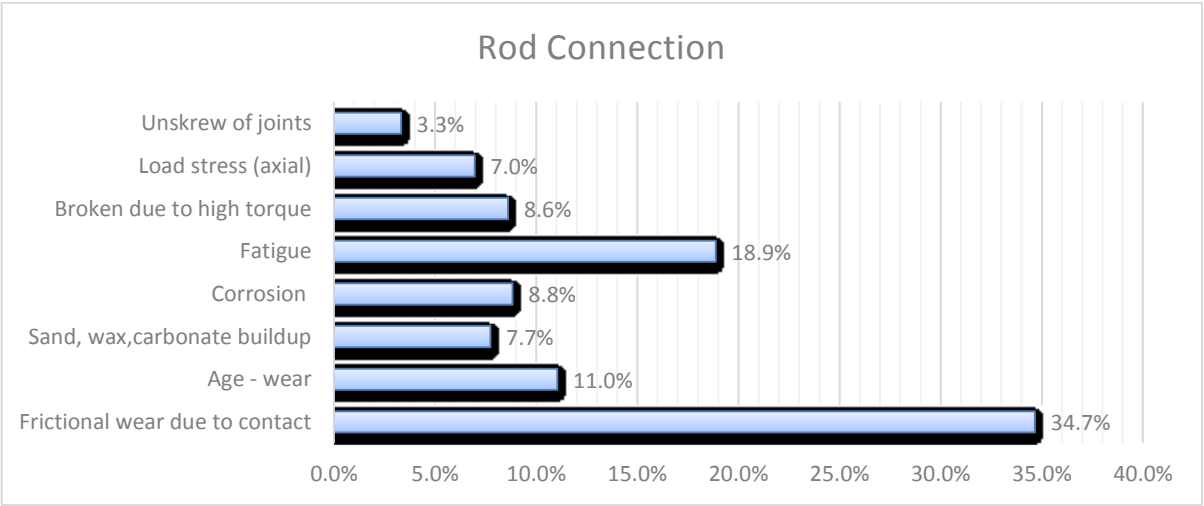

Figure 5.5: Rod Connection Failure Distribution within OMV Petrom in 2016

As opposed to the previous graph, Fig. 5.6, portraying rod body replacement reasons, peaks in the normal wear region, suggesting a rather uniform degradation of the rods. This incorporates the reduction of cross-sectional area of the rods, slight corrosion and erosion, implying an overall condition of the rods that cannot be used anymore.

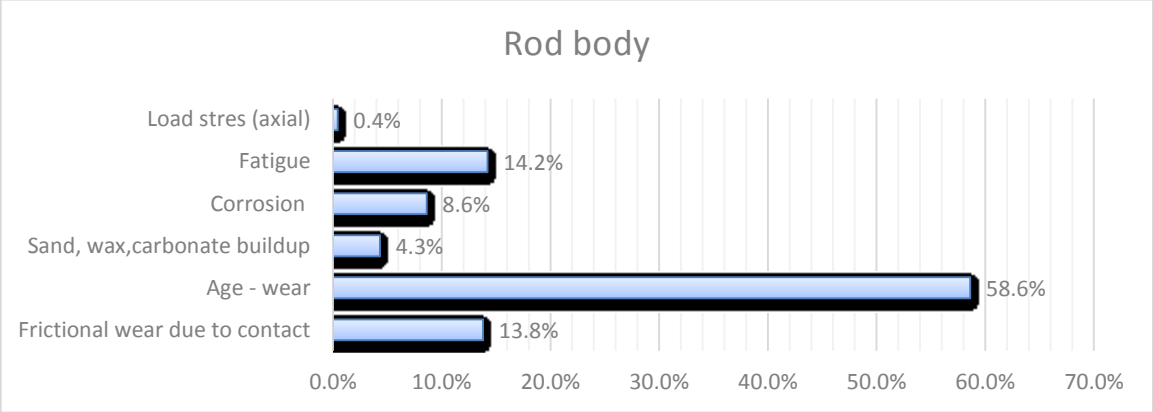

Figure 5.6: Rod Body Failure Distribution within OMV Petrom in 2016

5.3 Impact of failures on Key Performance Indicators

The operational capacity of the sucker-rod pumping system is affected when the system design is not optimal, or a proper maintenance program is not in place, resulting in premature equipment failure and downtime. Aside from the costs related to replacement of the failed equipment and interventions, malfunctions will lead to a loss of revenue associated with deferred production.

As a proactive measure to reduce the occurrence of failures and improve the reliability of the pumping operations, OMV Petrom initiated an equipment inspection and replacement program on the sucker-rod pumped wells within 2009 and 2010, which was followed by an appreciable reduction in the number of failures in the following years (Fig. 5.7). The improvements were sustained by continuous automatization of a considerable number of wells, which allowed monitoring and optimizing the wells' operation in real time. Consequently, one of the main performance indicators of the company, MTBF, defined as the ratio of the total uptime for a period and the number of stops during the same period, improved considerably. From 728 days in 2010 to 1655 days in 2016, the MTBF went up by about 130%, considering a population of 6400 wells equipped with a sucker-rod pumping system, highlighting the benefits of the maintenance measures implemented.

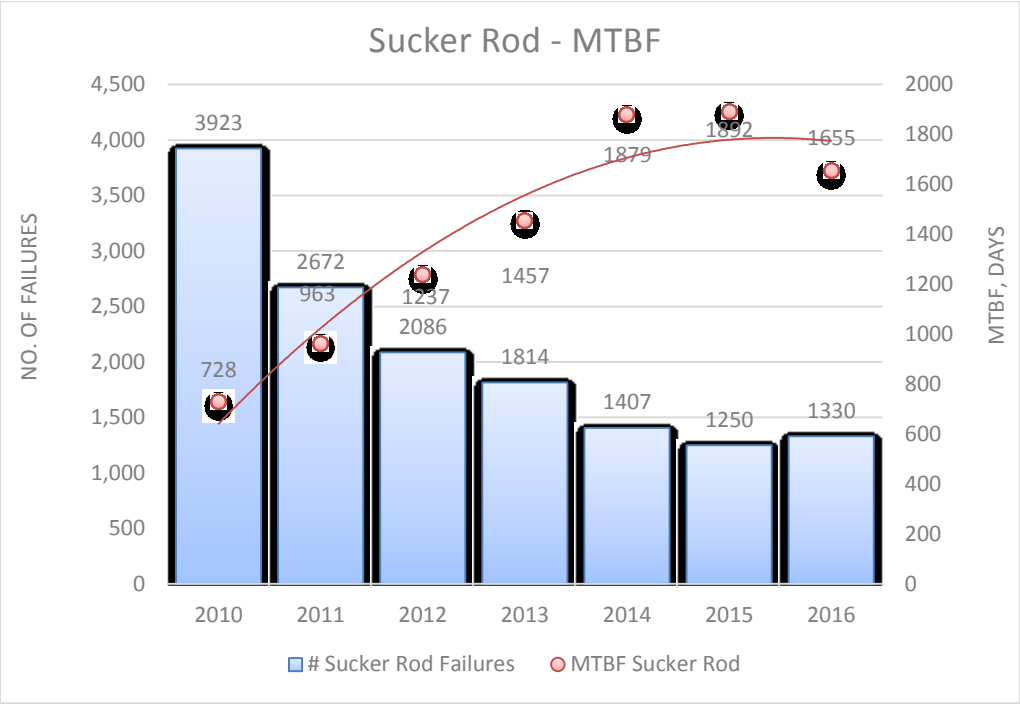

Figure 5.7: MTBF dynamics in OMV Petrom over the last 7 years

6 TOPSIS analysis

The TOPSIS model (Technique for order preference by similarity to ideal solution), has been developed by Hwang and Yoon in 1981. The concept of the model embodies the idea of the shortest Euclidian distance between the chosen solution and the ideal solution and, simultaneously, taking into consideration that the chosen solution is farthest from the negative ideal solution [23, pp. 11-13].

The ideal solution, and the negative ideal solution, are hypothetical solutions for which all alternatives relative to criteria attribute values correspond to the maximum and minimum attribute values in the database, respectively. Thus, the TOPSIS solution would not only be closest to the hypothetically best, but also the furthest from the hypothetically worst alternative.

The stepwise procedure of the best alternative selection is described as follows:

1. Define the quality criteria based on which the alternative methods will be graded. In this case, the chosen criteria are described in the table 6.1.

Table 6.1: Quality Criteria for the TOPSIS analysis

Quality Criteria	**Description**
Setting depth	The precision and applicability of the sucker-rod string design method based on the pump setting depth
Pumping speed	The precision and applicability of the sucker-rod string design method based on the pumping speed and susceptibility to the resulting acceleration forces
Inclination	The precision and applicability of the sucker-rod string design method based on the wellbore inclination and relative tortuosity
Complexity	The precision of the sucker-rod string design method based on the number of simplification assumption used and the forces considered in calculation
Flexibility	The possibility to operate with complex string designs, including recent technologies on the market
Safety	The relative range of stresses calculated by the method, considering the optimum balancing of the loads along the string, the risk of buckling occurrence and tensile failure
Economic	The cost of the resulted sucker-rod string based on the given design methods, considering the SF (service factor)
Cost	The methods' cost and availability

2. Allocate suitable grades (from 1 to 10) for the alternatives for each of the previously defined criteria (a better performance would indicate a higher mark). For the rod string

design methods comparison, the marks were determined according with the conclusion of the previous chapters and are presented in the table 6.2.

Table 6.2: TOPSIS ranking of the sucker-rod design methods based on the defined criteria

Method	Setting depth			Pumping speed			Inclination		
	< 1000 m	< 2000 m	> 2000 m	2 - 4,5 spm	4,5 - 8 spm	> 8 spm	0º	< 5º	> 5º
West	10	5	3	9	6	3	10	5	1
Neely	10	5	3	9	5	2	10	5	1
Gabor Takacs	10	8	5	10	8	6	10	7	5
OMV Petrom	10	5	3	9	6	3	10	6	3
RODSTAR	10	10	9	10	9	7	10	10	8

Method	Complexity	Flexibility	Safety	Cost	Economic
West	5	5	4	10	7
Neely	5	5	5	10	4
Gabor Takacs	8	9	7	10	10
OMV Petrom	6	5	3	10	6
RODSTAR	10	7	8	4	5

3. A decision matrix is build, given the number of alternatives and the number of criteria as the number of matrix rows, *N,* and matrix columns, *M,* respectively.
4. The matrix is normalized based on the quality criteria marks. The normalized matrix, R_{ij}, can be represented as [25, pp. 32-35]:

$$R_{ij} = \frac{m_{ij}}{\left(\sum_{j=1}^{M} m_{ij}^2\right)^{\frac{1}{2}}} \tag{6.1}$$

5. The normalized matrix is weighted based on the relative importance of the specific quality criteria with respect to the design method decision making. For this scope, a set of weights, w_j, is developed, such as $\sum w_j = 1$. The weighted normalized matrix, V_{ij}, is hence expressed as:

$$V_{ij} = w_j R_{ij} \tag{6.2}$$

The weights chosen for the scope of this thesis are presented in the table 6.3

Criterion	Setting depth	Pumping speed	Inclination	Complexity	Flexibility	Safety	Cost	Economic
Weight	0,15	0,15	0,15	0,1	0,1	0,2	0,05	0,1

6. The ideal and the negative ideal solution for each criterion is then calculated as:

$$V^+ = \left\{\left(\sum_i^{max} V_{ij}, j = 1,2,\dots,N\right), i = 1,2,\dots,N\right\} = \{V_1^+, V_2^+, \dots, V_M^+\} \tag{6.3}$$

$$V^- = \left\{\left(\sum_i^{min} V_{ij}, j = 1,2,\dots,N\right), i = 1,2,\dots,N\right\} = \{V_1^-, V_2^-, \dots, V_M^-\} \tag{6.4}$$

7. The overall performance of the design methods is determined by their Euclidian distance from $V_j{}^+$ and $V_j{}^-$ as follows:

$$S_i^+ = \left\{\sum_{J=1}^{M}\left(V_{ij} - V_j^+\right)^2\right\}^{0.5} \quad (6.5)$$

$$S_i^- = \left\{\sum_{J=1}^{M}\left(V_{ij} - V_j^-\right)^2\right\}^{0.5} \quad (6.6)$$

8. The relative closeness of a particular alternative to the ideal solution, P_i in %, can be expressed as:

$$P_i = \frac{S_i^-}{(S_i^+ + S_i^-)} \cdot 100 \quad (6.7)$$

The higher the P_i value, the better is the choice for a given situation.

For example, the best design method for a shallow well, with low pumping speeds, would be the Gabor Takacs method, as per Fig. 6.1.

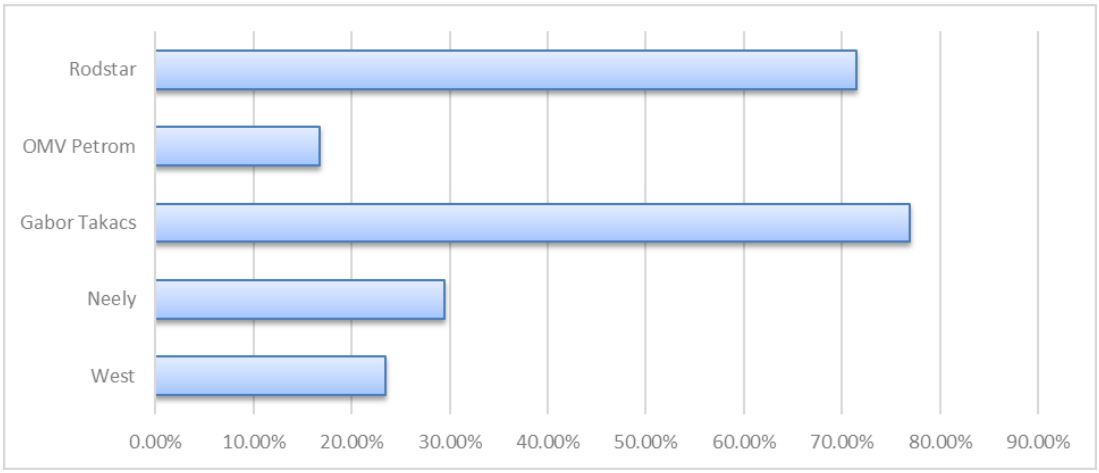

Figure 6.1: The TOPSIS analysis results for a shallow well application

For a deeper well, with higher pumping speeds and a crooked trajectory, the best method for the sucker rod string design would be RODSTAR (Fig. 6.2).

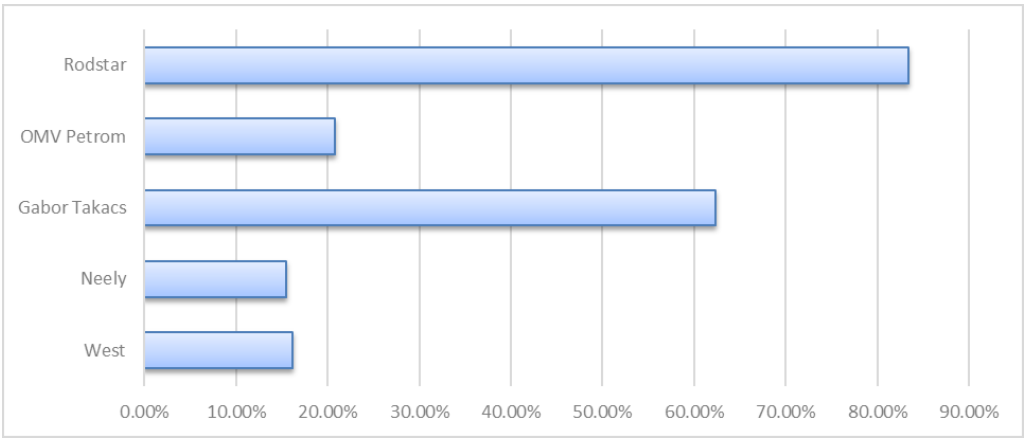

Figure 6.2:The TOPSIS analysis for a deep, inclined well application

After a trial of a range of various well conditions, the TOPSIS analysis would result in only two preferred design methods: RODSTAR – mainly for wells with a non-vertical trajectory and/or rod design which include special rod types (fiberglass and continuous rods), and Gabor Takacs – mainly for simple designs and well trajectories with very little to no deviation.

7 Conclusion

Sucker Rod Systems will continue to be the preferred used Artificial Lift System method in OMV Petrom, given the company's history and knowledge related to it. Therefore, system's design and optimization in order to further reduce the operating costs and increase the Meantime Between Failure (MTBF) is still a key exercise. This Master Thesis' investigation of the design goals of different models now used in the industry reveals huge differences in their basic principles, emphasizing the need of a proper decision matrix when it comes to the selection of the best available method.

The Bethlehem design model results in string designs with the same maximum stresses at the top of each taper. Lower tapers (with lower minimum stresses) have a higher service factor and lie closer to the allowed stress line if plotted on the Modified Goodman diagram. The fatigue loading on lower tapers is, therefore, higher, and these are more likely to experience premature failure. Setting the service factors equal in each taper, as done by West (1973), Gault and Takacs (1990) and Takacs and Gajda (2014) ensures the same level of safety in every taper section and no weak points. Neely's approach (1976) of setting the "modified stress" equal at the top of each taper, would mean that this design will generate different safety factors for each taper, upper tapers being more loaded than the lower ones. OMV Petrom's method relies on a non-sophisticated approach when it comes to the estimation of the dynamic loads, which, improved in time, has shown reasonably good results for the pool of wells currently in operation. Given that most of these wells have a non-crooked trajectory, low to medium pumping depths and relatively low fluid loads, the method has proven a viable and simple to operate algorithm for these specific conditions. However, when plotted on the modified Goodman diagram it proves to generate different service factors for each taper, therefore resulting in an unbalanced sucker rod string design.

Design calculation results, performed on two wells which define the average operating conditions for the region, along with plotted stresses on the Modified Goodman Diagram follow the general conclusions above, and provide a descriptive picture of the methods' differences. While RODSTAR method results in a design with relatively high service factors, which, though economical, might prove riskier, the OMV Petrom's method lies on the other side of the spectra with conservative service factors, which could result in an oversized sucker rod string and higher initial expenses for the equipment.

West's method taper lengths are fairly average in comparison with the other methods, but the minimum stresses of these tapers are largely higher than the average results given by other methods. Overestimation of the minimum stresses might lead to taper string design prone to buckling, therefore, this risk should be considered when using this design method. RODSTAR's results, on the other hand, tend to consider the widest range of rod stresses, having lower minimum stress results and higher maximum stress results compared to the rest of the methods. This might suggest good stress approximation, and consideration of a wider range of factors that can influence the rod stresses. OMV Petrom's method results trigger a much narrower range of stresses with significantly lower minimum and maximum stresses

compared to the other methods, which might be caused by an underestimation of the forces acting on the string and an overall increased level of tensile rod failure.

Given the methods' performance, the decision matrix reflects the obvious drawbacks and/or advantages of the approaches. However, for a specified set of well conditions, the choice will mainly follow two options: RODSTAR – for wells that have a more crooked trajectory, and include special types of rods, and Gabor Takacs for the wells with a simple trajectory, which do not require special design configuration.

8 References

[1] L. Firu, V. Manolache, F. Mocanescu și P. Chitu-Militaru, Extractia Titeiului prin Pompaj cu Prajini, Bucharest: Editura Didactica si Pedagogica , 2004.

[2] T. P. Gabor, Sucker-Rod Pumping Handbook. Production Engineering Fundamentals and Long-Stroke Rod Pumping, Petroleum Engineering Department, University of Miskolc, Hungary: Elsevier, 2015.

[3] P. West, “Improving Sucker Rod String Design,” *Petroleum Engineer,* no. July, 1973.

[4] A. Neely, “Sucker Rod String Design,” *Petroleum Engineer,* no. March, 1976.

[5] American Petroleum Institute, API RP 11L Recommended Practice for Design Calculations for Sucker Rod Pumping Systems (conventional units), Washington, D.C.: American Petroleum Institute, 1988.

[6] R. Gault and G. Takacs, “Improved Rod String Taper Design. Paper SPE 20676,” in *65th Annual Technical Conference and Exhibition of the SPE*, New Orleans, Louisiana, 1990, September 23-26.

[7] Theta Oilfield Services , User Manual RodStar - D/V, La Habra (CA), 2006.

[8] Wikimedia Commons, “Pump Jack - labelled,” 8 November 2015. [Online]. Available: https://upload.wikimedia.org/wikipedia/commons/5/5c/Pump_Jack_labelled.svg. [Accessed 2 March 2017].

[9] G. Boyun, L. Xinghui and T. Xuehao, Petroleum Production Engineering, A Computer-Assisted Approach, Elsevier Inc., 2007.

[10] A. Lubinski and K. Blenkarn, “Buckling of Tubing in Pumping Wells, Its Effects and Means for Controlling It,” *Trans. AIME,* no. 210, 1957.

[11] API Spec. 11B. Specification for Sucker Rods, Polished Rods and Liners, Couplings, Sinker Bars, Polished Rod Clamps, Stuffing Boxes, and Pumping Tees, Dallas (Texas): American Petroleum Institute, 2011.

[12] “EC21. Global B2B Marketplace,” [Online]. Available: http://www.ec21.com/product-details/Sucker-Rod---Different-Grade--9294913.html. [Accessed 06 March 2017].

[13] K. Carstensen, “Connectable rod system for driving downhole pumps for oil field installations”. United States of America Patent 7,108,063, 1996.

[14] T. Francisco Diaz Telli, “Increasing Sucker Rods' Working Capacities,” *JPT,* no. January, 2010.

[15] Weatherford, *COROD® Continuous Rod and Well Services,* 2013-2014.

[16] M. Reynolds, “Fiberglass Sucker Rod Design Considerations,” *The Journal of Canadian Petroleum Technology,* vol. 27, no. 5, 1988.

[17] S. Gibbs, Rod Pumping. Modern Methods of Design, Diagnosis and Surveillance, USA: BookMasters Inc., 2012.

[18] S. Gibbs, “Predicting the Behavior of Sucker-Rod Pumping Systems,” *Journal of Petroleum Technology,* vol. 15, no. 07, July 1963.

[19] S. Gibbs, “Design and Diagnosis of Deviated Rod-Pumped Wells,” *Journal of Petroleum Technology,* vol. 44, no. 07, July 1992.

[20] G. M. Takacs G., “An Enchanced Model for the Design of Tapered Sucker-Rod Strings,” *SPE Production & Operation,* no. February, 2017.

[21] API, *Recomended Practice for the Care and Handling of Sucker Rods - API 11BR,* API, 2008.

[22] Bethlehem Steel Company, Sucker Rod Handbook, Pennsylvania , 1953.

[23] H. A. Tripp, “Mechanical Performance of Fiberglass Sucker-Rod Strings,” *SPE Production Engineering,* no. August, 1988.

[24] M. Alemi, H. Jalalifar, G. Kamali and M. Kalbasi, “A prediction of the best artificial lift method selection on the basis of TOPSIS model,” *Journal of Petroleum and Gas Engineering,* vol. 1, no. 1, pp. 9-15, 2010.

[25] R. Rao, Decision Making in the Manufacturing Environment. Using Graph Theory and Fuzzy Multiple Atribute Decision Making, Springer-Verlog, 2007.

[26] C. Hwang and K. Yoon, Multiple Attribute Decision Making: a state of the art survey, Springer-Verlog, 1981.

Index

- A - cross-sectional area of a rod element
- a_i - instantaneous acceleration of the rod element at the moment i
- A_n - cross-sectional area of the top rod
- b,$\left(1-\frac{\rho_L}{\rho_S}\right)$ - buoyancy factor
- c - viscous damping factor
- E - Young's modulus of elasticity of the rod material
- f - Mills acceleration factor
- F_0, F_L - fluid load on plunger
- F_C - Coulomb mechanical friction forces between the rods and the tubing
- $F_{in,i}$ - inertial force in the string at the moment i
- F_{du}, F_{dd} - dynamic load components on the upstroke and downstroke
- F_{min}, F_{max} - minimum and maximum polished rod loads
- F_{ST} - the total static force acting on the polished rod
- g_c - gravitational constant
- I_{ai} - moment of inertia of articulating elements
- I_t - total rotary moment of inertia
- k_f, k_s - stiffness of the fiberglass section and of the steel section of the sucker rod string
- k_t - tubing stretch factor
- L, L_{total}- length of the taper section or pump setting depth
- L_u - unanchored tubing length
- M_{cb} - maximum counterbalance moment
- $MPRL$ - minimum polished rod load
- m_{up}, m_{down} - upstroke and downstroke kinematic coefficients
- n - pumping speed
- P - pitman length
- $PPRL$ - peak polished rod load
- R - crank shaft radius
- R_0 - overall speed ratio
- S - displacement of the sucker rod string
- S_a - fatigue endurance limit (allowable stress)
- SF - service factor
- SF_{act} - actual service factor
- S_{max} - maximum stress in taper string
- S_{min} - minimum stress in taper string
- S_{mod} - the modified stress
- t - time
- T_a - minimum tensile strength of the rod material
- T_{ai} - articulating inertia torque
- T_{cb} - counterbalance torque

- T_m - prime-mover torque
- T_{rod} - rod-load torque
- t_{tvc} - traveling valve closing time
- v_s - sound velocity in the rod material
- W - weight of the rod string in air
- w_{avg} - average rod string weight
- w_r - average weight of the taper section
- W_{rf} - buoyant rod string weight
- γ_L - specific gravity of the liquid
- $\frac{\partial u}{\partial x}$ - rod strain
- θ - crank angle
- λ - sucker-rod string elongation
- ξ - beam angle
- ρ_s - density of the rod material
- ρ_L - fluid density
- σ_o fatigue resistance in a pulsating stress cycle
- σ_{-1} - fatigue resistance in case of an alternative symmetrical stress cycle
- σ_m, - mean stress of a stress cycle
- σ_v variance of the stress from the mean
- σ_t - tensile strength of the material
- σ_y - yield point of the material in static conditions
- τ - counterbalance phase angle

Appendices

Appendix A: Sucker rod design simulation results

Well nr 1

Table 0.1: Well operational data

Pump setting depth	*4100,3 ft*	**Plunger diameter**	*1,75 in*
PR stroke length	*146,85 in*	**Pumping speed**	*5,8 SPM*
Rod grade	*Grade D*	**Service factor**	*0,9*
API rod code	*76*	**Liquid Specific Gravity**	*1,036*

Table 0.2: Sucker-rod string design results

Method	**Parameter / Rod diameter**	**Length, ft**	**Smin, psi**	**Smax, psi**	**SF**
West	**7/8**	1602	11811	20962	0.572
	3/4	2498	8542	19883	0.571
Neely	**7/8**	1589	7068	22634	0.666
	3/4	2511	4030	20873	0.646
Gault Takacs	**7/8**	1510	8843	21493	0.614
	3/4	2590	6773	20839	0.616
OMV Petrom	**7/8**	1656.5	6322	14035	0.418
	3/4	2444	4462	13429	0.413
RODSTAR	**7/8**	1575	6653	23398	0.693
	3/4	2525	3468	21455	0.671

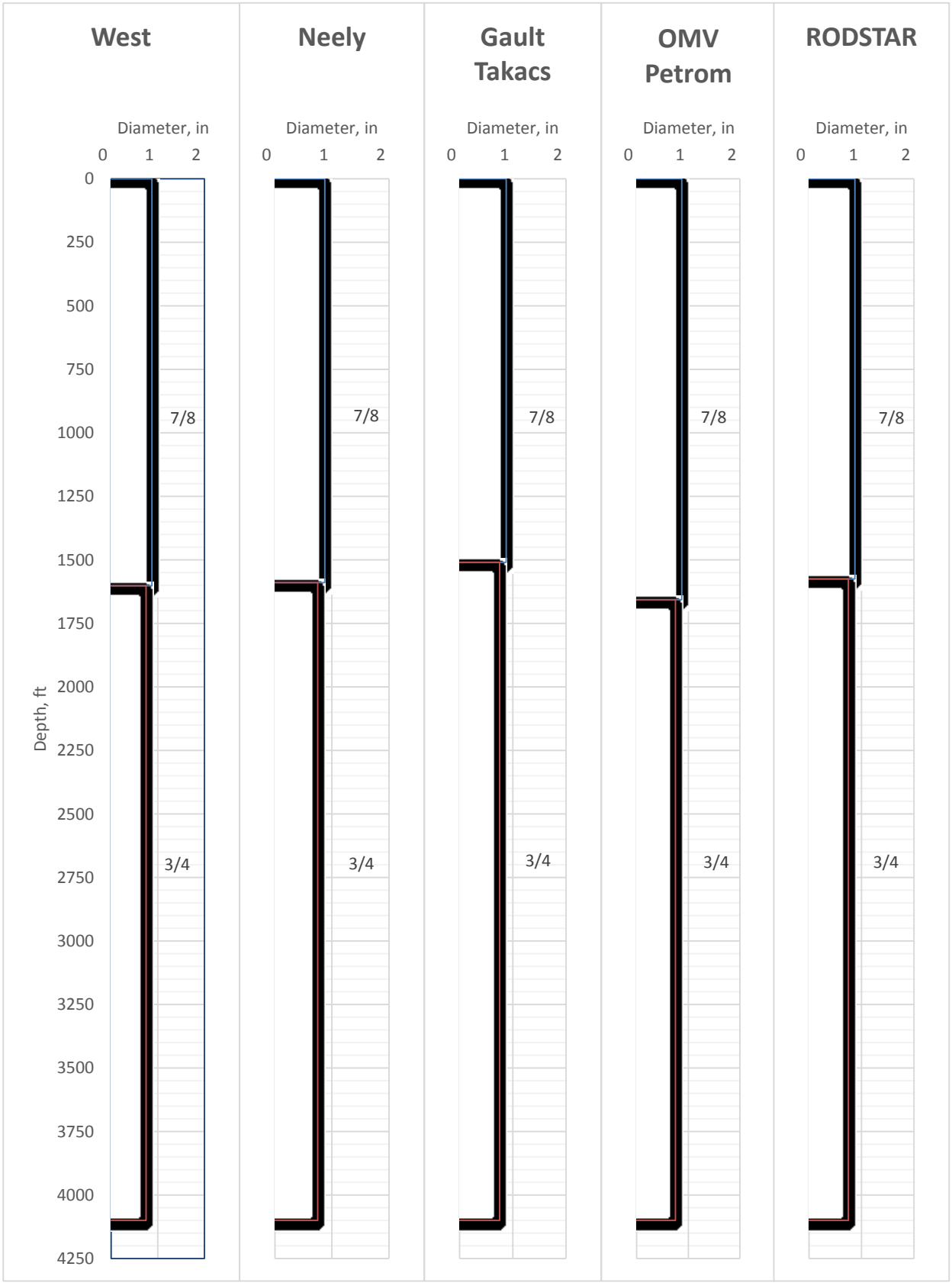

Figure 0.1: Sucker-rod string design diagram

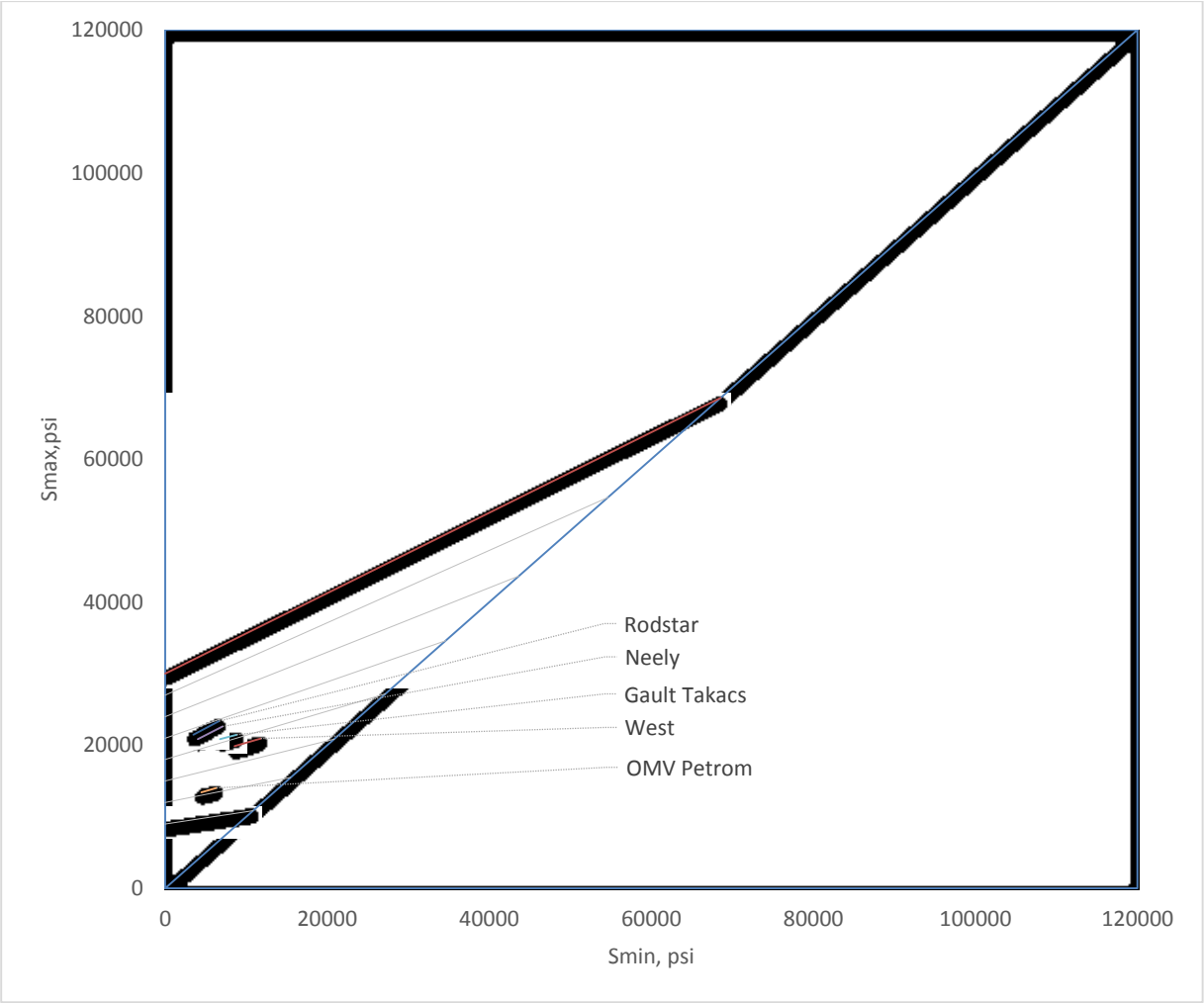

Figure 0.2: Rod stresses for well 1 plotted on the modified Goodman diagram given by different design methods

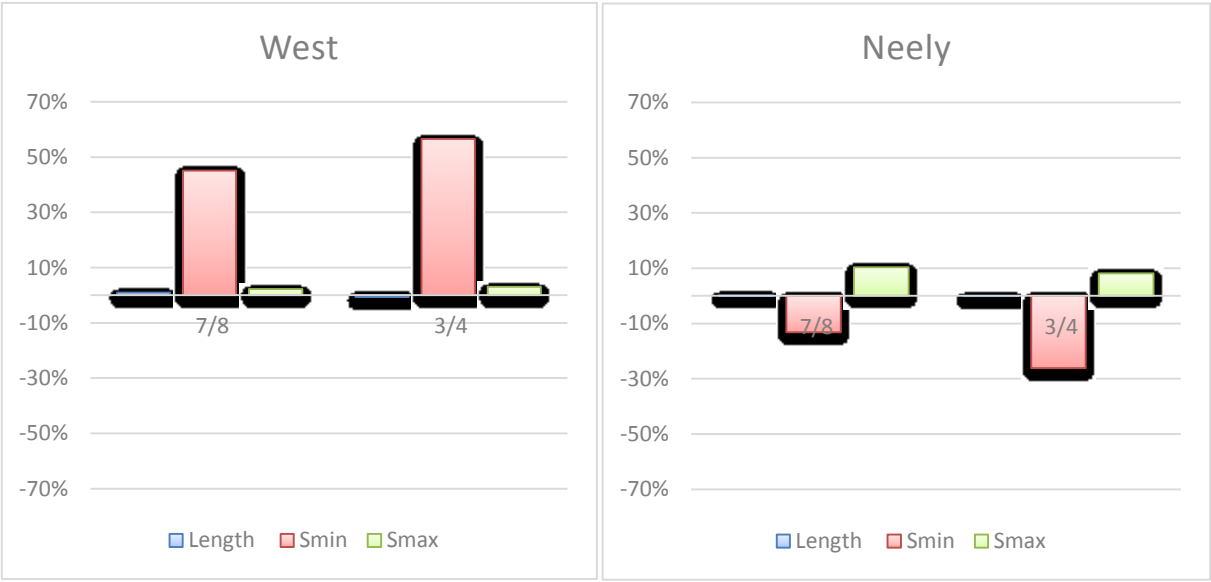

Figure 0.3: Relative length of the sucker rod string tapers, compared with the main stresses - comparison of design methods

Well nr 2

Table 0.3: Well operational data

Pump setting depth	*7523,6 ft*	**Plunger size**	*1,25 in*
PR stroke length	*124,5 in*	**Pumping speed**	*3,6 SPM*
Rod grade	*Grade D*	**Service factor**	*0,9*
API rod code	*75*	**Liquid Specific Gravity**	*1,007*

Table 0.4: Sucker-rod string design results

Method	Parameter / Rod diameter	Length, ft	Smin, psi	Smax, psi	SF
West	**7/8**	2192	19829	27465	0.667
	3/4	2535	16176	26050	0.666
	5/8	2796	10100	23698	0.664
Neely	**7/8**	2407	16577	26780	0.681
	3/4	2658	11562	23910	0.655
	5/8	2459	4682	20043	0.614
Gault Takacs	**7/8**	2184	16272	26227	0.670
	3/4	2526	13289	25060	0.669
	5/8	2813	8328	23119	0.667
OMV Petrom	**7/8**	2217	10920	16898	0.467
	3/4	2582	8768	15498	0.443
	5/8	2726	5204	12969	0.393
RODSTAR	**7/8**	2425	14586	27951	0.731
	3/4	2675	9470	24695	0.699
	5/8	2424	2655	20204	0.642

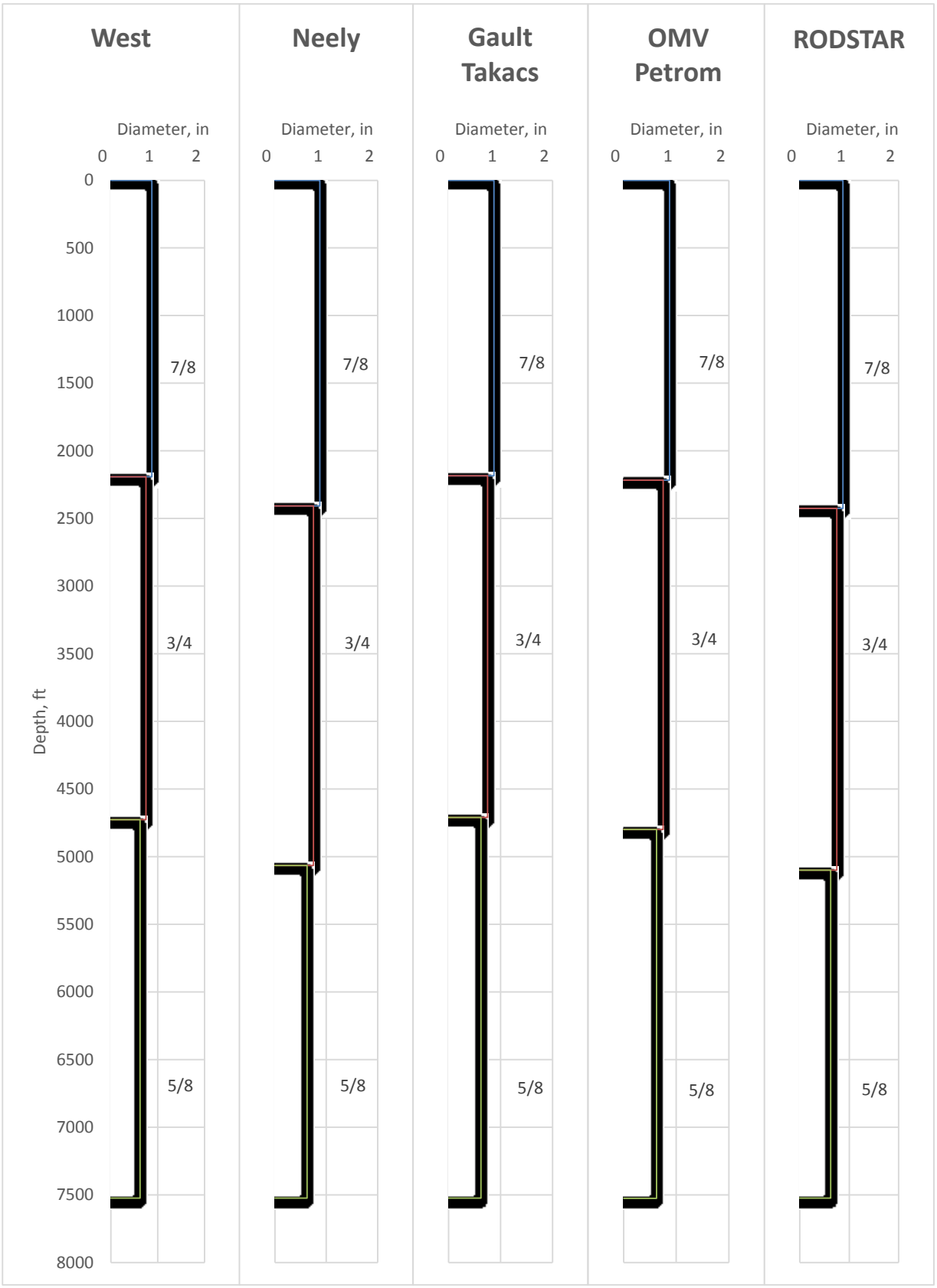

Figure 0.4: Sucker-rod string design diagram

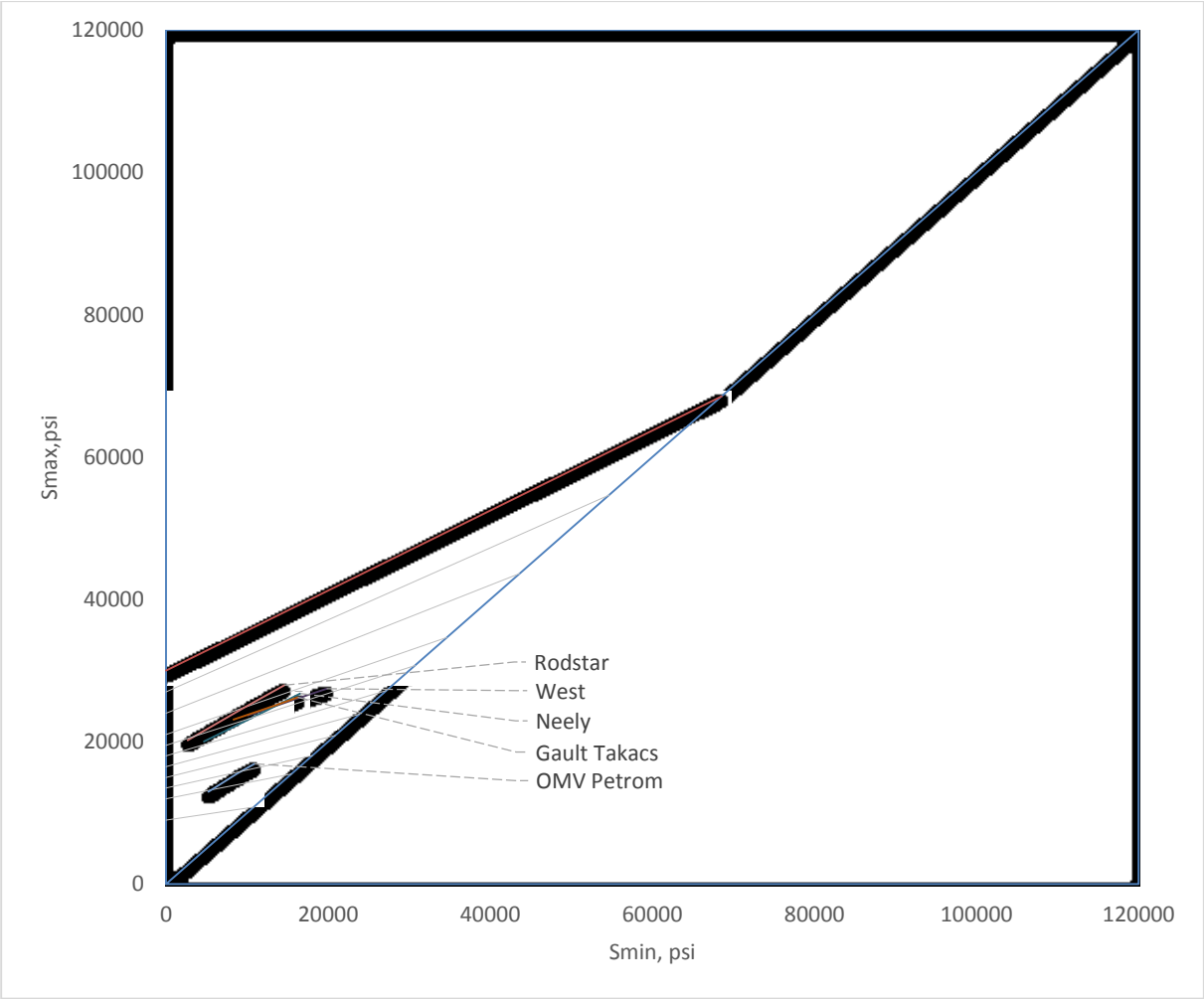

Figure 0.5: Rod stresses for well 1 plotted on the modified Goodman diagram given by different design methods

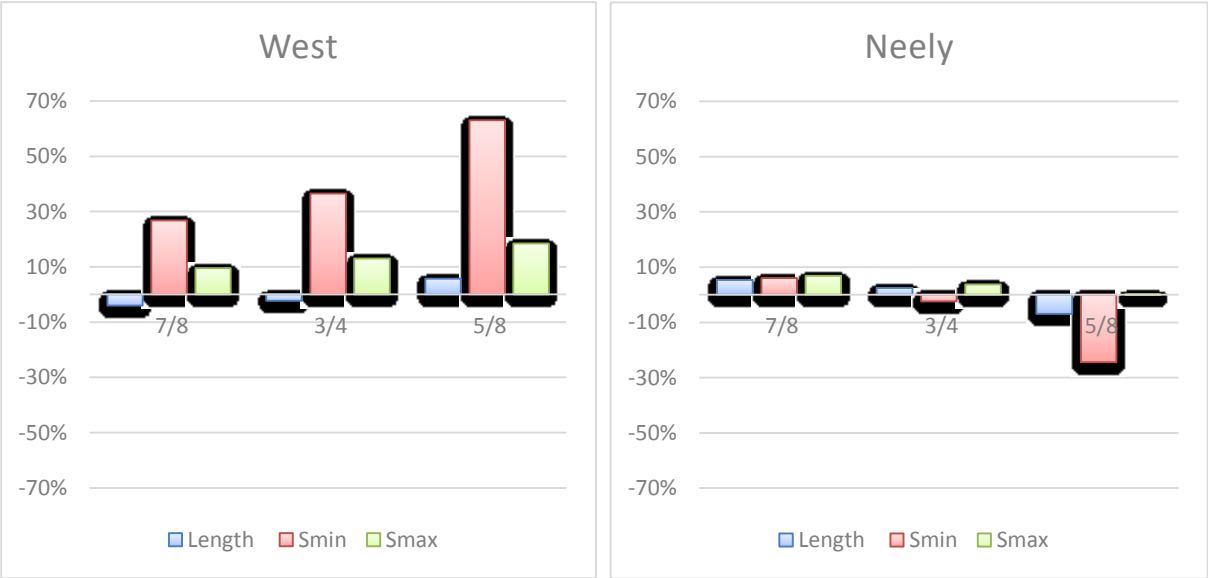

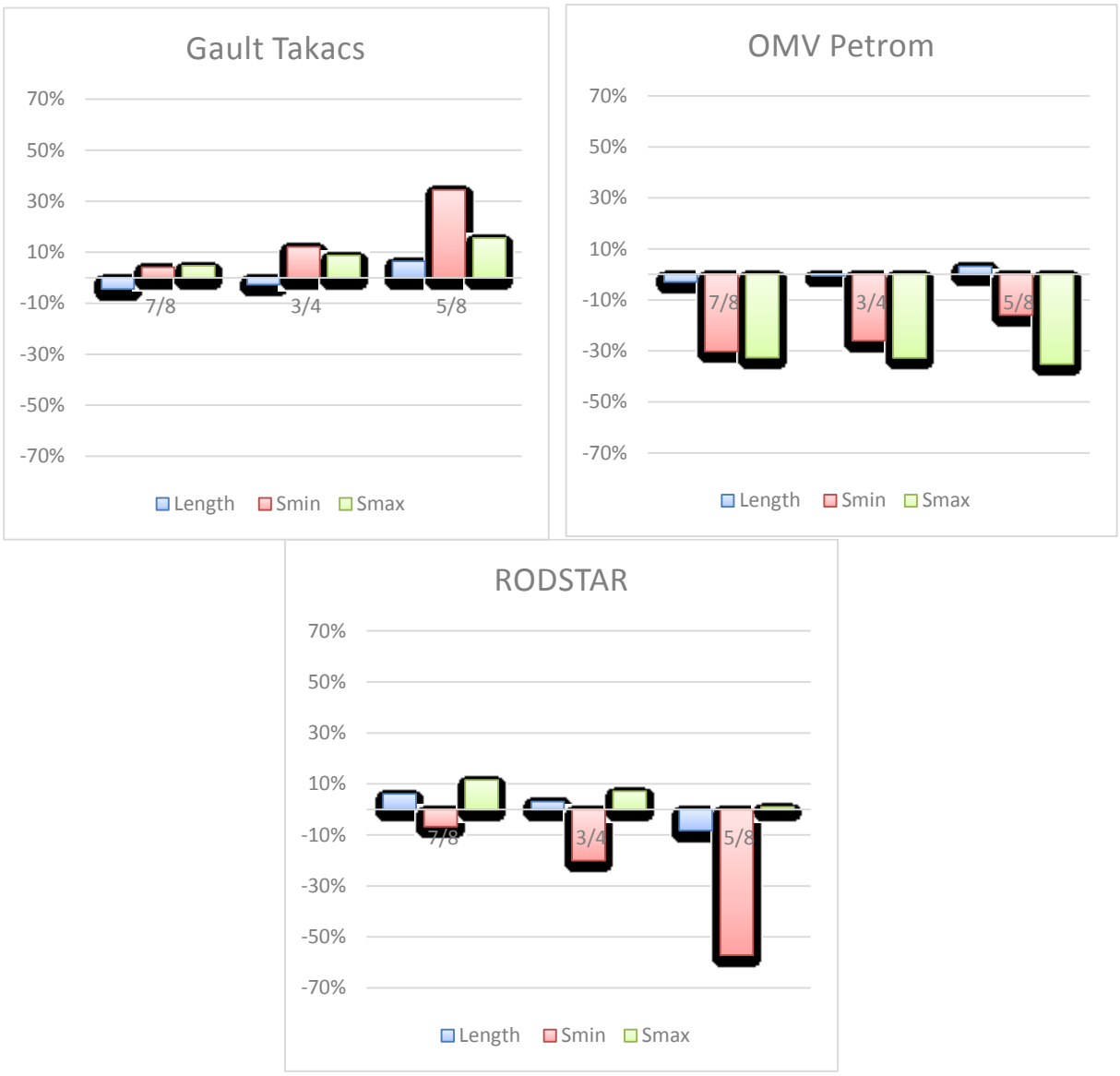

Figure 0.6: Relative length of the sucker rod string tapers, compared with the main stresses - comparison of design methods